Antal Kerpely Doctoral School of Materials Science and Technology

Innovative Development and Investigation of Doped and Cu-Composite $BaTiO_3$ Materials for Advanced Multilayer Ceramic Capacitors

Thesis Booklet

By
Mohammed Tihtih

Supervisor:
Dr. István Kocserha, Associate Professor

Head of the Doctoral School
Prof. Dr. Valéria Mertinger

Institute of Ceramic and Polymer Engineering

Faculty of Materials and Chemical Engineering

University of Miskolc

Miskolc, Hungary

2024

Abstract

Electroceramics are necessary component in modern technologies of many kinds. In this regard, barium meta-titanate ($BaTiO_3$ or BT) based materials with ABO_3 perovskite structure are potential candidates for applications in electronic devices because of their piezoelectric, ferroelectric, and optical properties. Barium titanate-based materials have attracted significant interest, due to their widespread applications in wireless communication, space and defense. Barium titanate based ferroelectric materials are suitable for these applications due to their electric field dependent permittivity (ε_r) and low dielectric loss (tan δ) above Curie temperature (Tc). Ferroelectric materials generally have high dielectric losses, which is due to piezoelectric grain resonance and domain wall motion.

This thesis investigates the synthesis, characterization, and properties of doped $BaTiO_3$ ceramics prepared using a modified sol-gel method. Various compositions including $BaTiO_3$, $Ba_{1-x}Sr_xTiO_3$, $Ba_{1-x}Y_xTiO_3$, $BaTi_{1-x}Y_xO_3$, $Ba_{1-x}Y_xTi_{1-x}Y_xO_3$, and $Ba_{1-x}Sr_xTi_{1-x}Y_xO_3$ (x=0.075) were successfully synthesized and characterized for their structural, microstructural, chemical compositional stoichiometry, optical, thermal conductivity, and mechanical properties. X-ray diffraction (XRD) and Rietveld refinement revealed the tetragonal structure of BT, BSrT, and BYT ceramics, while BSrTY, BTY, and BYTY samples exhibited a cubic structure. Fourier-transform infrared spectroscopy (FT-IR) supported the XRD analysis and scanning electron microscopy (SEM) indicated the formation of particles in flat block shapes. Energy-dispersive X-ray spectroscopy (EDS) confirmed the high purity of the ceramic samples. The thermal conductivity changes induced by Y and Sr dopants were attributed to alterations in Ti-O bond distances and bond strengths. UV-vis spectroscopy identified a decrease in the optical band gap due to oxygen vacancies and lattice distortions. Mechanical strength analysis revealed a correlation between dopant content and compressive strength, with undoped $BaTiO_3$ exhibiting the highest strength. Additionally, dense BST-Cux ceramic composites were fabricated using spark plasma sintering, demonstrating enhanced AC conductivity with increasing Cu content and temperature. Electrical conductivity mechanisms shifted from oxygen vacancy migration to band conduction, and dielectric behavior varied based on phase ratio, with composites displaying elevated permittivity at low frequencies. These findings provide insights into the defect structure and thermoelectric behavior of doped $BaTiO_3$ ceramics, contributing to their potential applications in micro-optical electro-mechanical systems and the multilayer ceramic capacitor (MLCC) industry.

1. Introduction

Barium titanate (BT) is a type of material that is often used in the electrical and electronic industries due to its various desirable properties, such as its ability to exhibit ferroelectricity, pyroelectricity, and piezoelectricity, as well as having a high dielectric permittivity and a positive temperature coefficient of resistivity. It is abbreviated as BT and is written as $BaTiO_3$ in chemical notation [1], [2]. Perovskite materials that are derived from barium titanate have a wide range of applications, including use in devices that have a positive temperature coefficient, devices that generate pulses, infrared detectors, microwave electronics that can be voltage-tuned, multilayer ceramic capacitors, piezoelectric and ultrasonic actuators, thermal sensors and controllers, and microwave devices that utilize piezoelectric transducers and charge storage devices[3-5] and so forth. To produce multilayer ceramic capacitors (MLCCs) using BT material, the formulation of the BT must be carefully designed to control its electrical properties, particularly at high temperatures and under high electric fields [6]. To improve the reliability of multilayer ceramic capacitors (MLCCs) made with BT, various additives and dopants, such as yttria (Y_2O_3), are substituted to the $BaTiO_3$.

Yttrium (Y) is added to barium titanate to improve the reliability of multilayer ceramic capacitors. The Y^{3+} ion has an ionic radius that is intermediate in size between the Ba^{2+} and Ti^{4+} ions, which allows it to occupy either the Ba^{2+} or Ti^{4+} site in the BT lattice [7]. This means that the Y^{3+} ion can act as an acceptor or donor depending on its position in the lattice, and its inclusion in the BT structure is influenced by kinetic and thermodynamic factors [8], [9]. It is reported that the formation energy of $Y_{\dot{B}a} + V''_{Ba}$is 7.23 eV whereas it is only 4.35 eV to form a $Y_{\dot{B}a} + V'''_{Ba}$ defect [10].

A rationally modified synthetic route can be adapted to prepare $BaSrTiO_3$–Cu (BST-Cu) composite powders. This involves developing a new synthetic route and an advanced sintering method to achieve a microstructure with homogeneously dispersed Cu in an ultrafine BST ceramic matrix. Efforts have focused on controlling the size and distribution of metal nanoparticles, but only micro composites have been reported so far. Uniformly distributed metal particles in a ceramic matrix are essential for good percolative ceramic–metal composites, a novel concept in dielectric materials. In this study, spark plasma sintering (SPS) successfully consolidated BST–Cu powders into composites with ultrafine microstructures. SPS offers fast heating rates, mechanical pressure, short sintering times, and low temperatures, promoting densification and reducing grain coarsening in nano or submicron-composite powders. [41-44].

This PhD work aims to optimize yttrium and strontium-doped barium titanate (BT) materials for improved performance in multilayer ceramic capacitors (MLCCs) and other electronics. By investigating dopant interactions with the BT lattice, the research seeks to enhance MLCC reliability through controlled material properties. The study involves experimental analysis of dopant incorporation, solubility, and their effects on structural, optical, and thermoelectric properties using advanced characterization techniques. Innovative synthesis methods and composite materials are explored to improve mechanical, electrical, and optical properties. Additionally, metallic particle composites are synthesized using spark plasma sintering (SPS) to optimize performance. This research advances BT-based materials, focusing on MLCC reliability and performance.

2. Summary of literature

Perovskites obtain their name from the calcium titanium oxide ($CaTiO_3$) structure which was first discovered in the Ural Mountains of Russia by Gustav Rose in 1839 and is named after a Russian nobleman and mineralogist Count Lev Aleksevich Von Perovski (1792–1856)[32].
Generally, perovskites have the general formula ABO_3 where, A and B are two cations of very different sizes and O is an anion that bonds to both[33]. A large number of perovskite type oxides have been studied because of their interesting properties including superconductivity, insulator-metal transition, ionic conduction characteristics[34], dielectric properties and ferroelectricity[35]. Perovskite is one of the most frequently encountered structures in solid-state physics, and it accommodates most of the metal ions in the periodic table with a significant number of different anions. During the last few years, many experimental and theoretical investigations were devoted to the study of perovskite solids typically ABO_3.
The physicochemical properties of these materials are dependent on the crystal structure, lattice defect, exposed lattice plane, surface morphology, particle size, and specific surface area as well as the pore structure[36]. Up to now, a large number of perovskite-type oxides and perovskite-like oxides have been generated and investigated for clarifying their physicochemical properties.
Recently, perovskite structured ceramics have become one of the worldwide materials due to their peculiar properties viz. ferroelectric, thermo-electric, pyroelectric, dielectric and optical properties. Depending on these peculiar properties perovskite ceramics have several extraordinary applications such as random access memories, tunable microwave devices, capacitors, displays, piezoelectric devices, sensors, actuators, transducers and wireless communications [37].

2.1 Barium titanate ($BaTiO_3$)

The discovery of ferroelectricity in barium titanate ($BaTiO_3$) has given birth to many ABO_3 type materials. The diversity of structures exhibited by $BaTiO_3$ based perovskites, continues to fascinate in a range of areas including solid state chemistry, physics, and the earth sciences [40]. $BaTiO_3$ is a white solid and typical ABO_3 perovskite-type material. It has four kinds of crystal systems: hexagonal, cubic, tetragonal, orthorhombic, and rhombohedral, depending on the phase transition temperature [41]. The basic crystalline structure of $BaTiO_3$ at above 130°C is the ideal cubic perovskite structure. Below Curie temperature $BaTiO_3$ is tetragonal. When the temperature is decreased further, the structure of $BaTiO_3$ gradually changes from tetragonal to orthorhombic, and finally to rhombohedral. In the cubic perovskite phase, the barium and oxygen ions together form a face-centered cubic lattice (fcc), with titanium ions positioned on octahedral interstices.

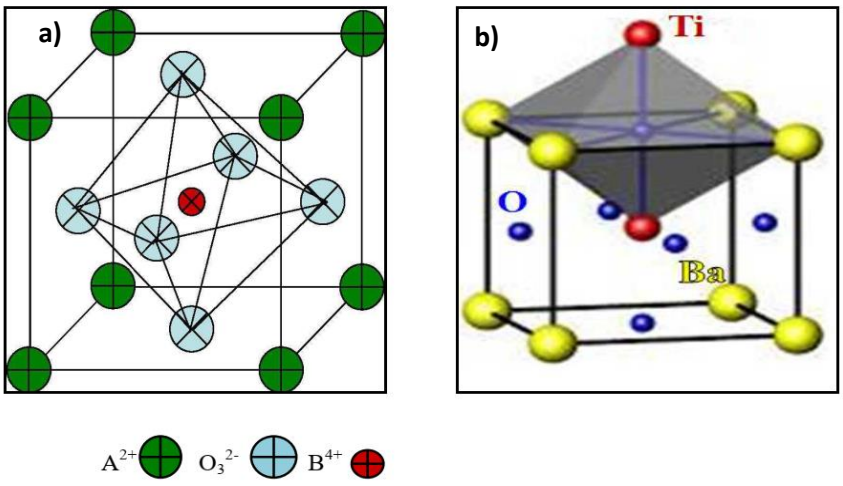

Figure 1. a) Perovskite Structure and b) Crystal Structure of $BaTiO_3$ [42]

Habib et al [41] finds the influence of temperature, aging time and particle size of titania precursor on the hydrothermal crystallization of $BaTiO_3$ and the morphological changes occurring during the formation of $BaTiO_3$ [41]. Hung et al adopted the sol–gel process along with the addition of a surfactant in order to get controlled sized and well-dispersed $BaTiO_3$ nanopowders [42].

2.2 Synthesis of $BaTiO_3$

Various methods have been employed to prepare $BaTiO_3$ materials, each with its unique advantages and applications. These methods include the molten salt method [43], sputtering [44], hydrothermal [45], solvo-thermal [46], which involve the use of both solvent and heat to drive chemical reactions, and sol-gel [47], where a solution precursor undergoes hydrolysis and condensation reactions to form a gel that can be further processed into desired forms. Amongst these methods, hydrothermal and sol-gel routes stand out as the most extensively employed for synthesizing $BaTiO_3$ nanoparticles. The hydrothermal method, leveraging aqueous solutions under controlled temperature and pressure conditions, offers superior crystallinity and phase purity even at relatively low temperatures. Similarly, sol-gel synthesis provides a versatile approach for tailoring the properties of $BaTiO_3$ nanoparticles, facilitating precise control over composition, particle size, and morphology. These methods collectively enable the production of $BaTiO_3$ nanoparticles with a highly crystalline structure and pure phases, essential for various technological applications.

2.3 Doping Barium titanate ceramics

The intentional introduction of impurities into a host lattice is the process known as doping [48] leading to novel phenomena very different from the precursor materials. Bulk semiconductors are successfully doped to build functional devices, and imparted by new electrical, optical, mechanical, and magnetic properties [49], [50]. crystalline semiconductors with unusual size-dependent optical and electronic behavior, however, are already marketed for applications as wavelength-tunable lasers, optical gain devices, bioimaging and solar cells [49]. Because their electronic states are confined to a small volume, doping nanocrystals results in phenomena not found in bulk materials.

Doping $BaTiO_3$ ceramics is of great importance in the fabrication of electric and electronic devices, and a large number of different dopants can be accommodated in the $BaTiO_3$ lattice. The ionic radius of dopants is the parameter which mainly determines the substitution site. For ions of the first series of the transition metals, like Cr^{3+}, Mn^{2+}, Mn^{3+}, Fe^{3+}, Co^{3+} and Ni^{2+}, it is well established that they preferentially substitute on the Ti^{4+} site.

2.4 Ceramic-Metal composites

Ceramic metal composites (CMCs) combine ceramic and metal phases to enhance properties and reduce costs. They offer improved strength, stiffness, hardness, wear resistance, and lower thermal expansion. Despite challenges like high processing costs and reduced ductility, recent advances are promising. By incorporating ductile reinforcements like particles and fibers, CMCs address ceramic brittleness, aiming to improve fracture toughness and reliability. Research focuses on minimizing flaws to enhance toughness and reliability. CMCs represent significant progress in material science, with interpenetrating composites offering unique structural advantages.

2.5 Spark plasma sintering (SPS)

Spark plasma sintering (SPS) is a rapid method for fabricating bulk materials from powders, offering fast heating, short holding times, and lower sintering temperatures compared to conventional methods. It's especially useful for nanostructured materials, composites, and refractory metals. Further research is needed to understand its mechanisms, including the role of spark plasma and discharge. Also known as field-activated sintering and pulsed electric current sintering, SPS allows fast heating rates (up to

1000 °C/min) and short holding times (0–15 min) at temperatures 200–300 °C lower than conventional techniques.[10-12]. Because of its great advantages, SPS is by far the most popular of the ultrarapid sintering techniques and is used to process nanostructured materials, amorphous materials, intermetallic compounds, metal matrix and ceramic matrix composites, highly refractory metals, and ceramics, etc., which are difficult to sinter by common methods [28-29].

Scholarly discourse commonly acknowledges that during the SPS process, a high electric–pulsed current is applied to the electrodes (as shown in Figure 2), and the microscopic electrical discharges in the gaps between the powder particles generate plasma, causing sintering [27]. The spark discharge can effectively eliminate adsorptive gas and any impurities present on the surface of the powder particles and can easily destroy the oxide films on the particle surface, leading to an enhancement of the thermal diffusion ability of the sintered material [28]. In addition, Joule heating and plastic deformation effects contribute to the densification of the powders.

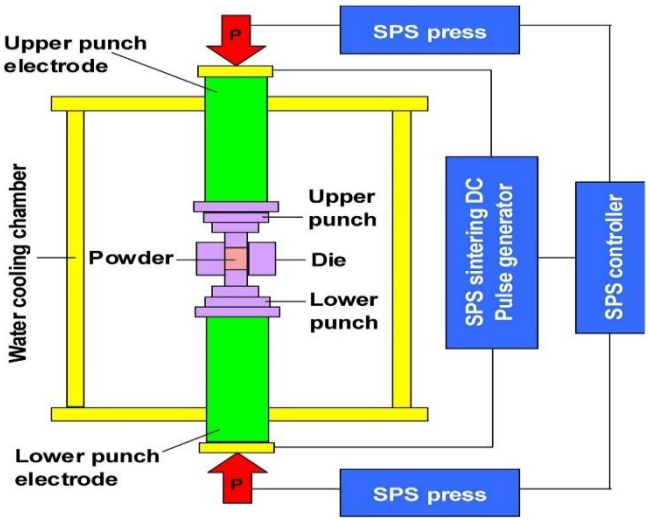

Figure 2. A schematic of the SPS process [110].

2.6 Knowledge gap

The literature review reveals a significant body of work on doped barium titanate synthesis and applications. However, the impact of dopants (Sr, Y) on $BaTiO_3$ composites, particularly on mechanical and thermoelectrical properties, remains unexplored. The sol-gel method, known for precise stoichiometry control, has not been extensively employed at lower temperatures using simple equipment for these investigations. Moreover, no studies have addressed the comparative influence of strontium and yttrium co-doping on the structural, microstructural, compressive strength, thermoelectrical, and optical properties of $BaTiO_3$ composites. This gap necessitates a comprehensive analysis focusing on major properties, emphasizing the stoichiometric ratio of $BaTiO_3$ and its semiconducting nature, especially concerning its application in multilayer ceramic capacitors (MLCCs). Additionally, the recent surge in interest surrounding ceramic-metal composites, due to enhanced permittivity and thermal conductivity near the percolation threshold, lacks detailed investigations into their electrical and thermal conductivity. Despite widespread studies on colossal permittivity in these composites, there is a notable absence of reports on the synthesis and spark plasma sintering of $Ba_{0.85}Sr_{0.15}TiO_3$-Cu composite powders, with no dedicated publication on the electrical, dielectric, and thermal properties of $Ba_{0.85}Sr_{0.15}TiO_3$-Cu ceramic composites. Closing these gaps is crucial for advancing our understanding of these materials and unlocking their potential applications.

2.7 Objectives

The primary objectives of this study are as follows:

1. Structural, Optical, and Thermoelectric Enhancement of BSrxT Ceramics:
   - Produce BSrxT ceramics with varying Sr concentrations (x=0, 5, 12.5, 15, 20, and 30%) using the sol-gel method.
   - Investigate the effects of Sr concentration on lattice parameters, crystalline phase, and microstructure through X-ray diffraction (XRD) and scanning electron microscopy (SEM).
   - Analyze compositional stoichiometry using energy dispersive spectrum (EDS) analysis.
   - Evaluate compressive strength properties as a function of Sr content and grain size.
   - Study thermal conductivity at room temperature.
2. Yttrium-Doped $BaTiO_3$ for Multilayer Ceramic Capacitors (MLCCs):
   - Prepare yttrium doped $BaTiO_3$ with various doping concentrations and sinter the materials in air.
   - Investigate structural, microstructural, thermoelectric, and optical properties, with a focus on stoichiometric ratio and semiconducting nature for MLCC applications.
3. Sr and Y Doped and Co-Doped $BaTiO_3$ Ceramics:
   - Utilize sol-gel technique to prepare BSrxT ceramics with formulas $BaTiO_3$, $B_{1-x}Sr_xTiO_3$, $Ba_{1-x}Y_xTiO_3$, $BaT_{1-x}Y_xO_3$, $Ba_{1-x}Y_xTi_{1-x}Y_xO_3$, and $Ba_{1-x}Sr_xTi_{1-x}Y_xO_3$ (x=0.075).
   - Investigate influences of Sr^{2+} and Y^{3+} ions on phase structure, lattice constants, and microstructure using XRD and SEM.
   - Identify compositional stoichiometry with EDS analysis.
   - Examine optical behavior through UV-visible spectroscopy.
   - Analyze compressive strength properties as functions of Sr and Y concentrations and grain size distribution.
   - Investigate thermal conductivity as a function of temperature.
4. Enhanced Electrical Properties with Copper incorporation:
   - Incorporate copper metal as reinforcement within the BST ceramic matrix to enhance electrical properties.
   - Evaluate the composite's characteristics as an innovative electrical material with applications in optoelectronics, microelectronics, and spintronics devices.

3. Preparation methods

3.1. Synthesis of $Ba_{1-x}Y_xTiO_3$ ceramics

BYxT (x=0-30%) ceramic samples were prepared using a sol-gel method. Barium acetate, yttrium acetate, and titanium isopropoxide were used as precursors, with lactic and acetic acids as stabilizing agents. The process involved dissolving titanium isopropoxide in water and acetic acid at 70°C, then stabilizing it with lactic acid. Barium and yttrium acetates were dissolved in water at 90°C and added to the titanium solution, forming a clear mixture at 80°C. This mixture was turned into a gel, dried, and processed to avoid agglomeration. The resulting xerogel was calcined at 950°C, pressed into pellets, and sintered at 1200°C for 6 hours with controlled heating and cooling.

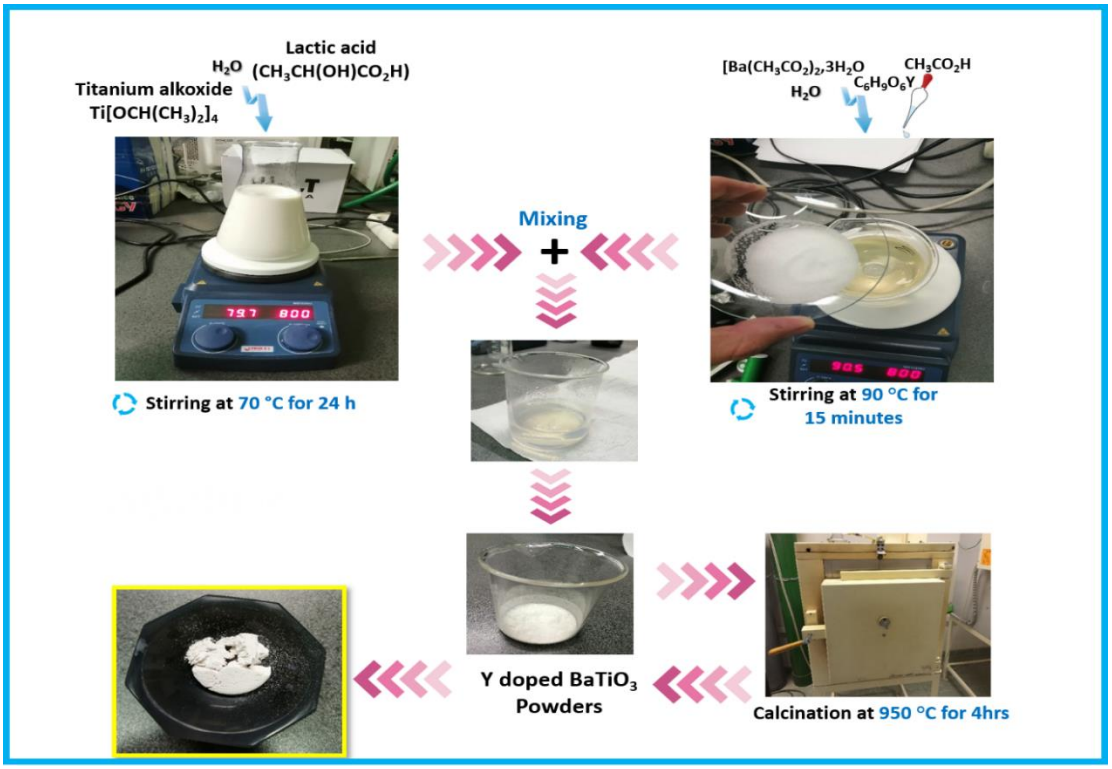

Figure 3. Synthesis flowchart of the ceramic materials

3.2 Preparation of BST-Cu and spark plasma sintering process

Barium strontium titanate (BST) powders were mixed with high-purity copper (Cu) powders (0-40 wt.%) using ball milling with ethanol and zirconia balls for 12 hours. The slurry was dried, and the mixed powders were extracted. To densify the BST-Cu composite, spark plasma sintering (SPS) was performed using a graphite die at Tallinn University of Technology. Powders (2-2.6 g) were heated under vacuum to 600°C, then at 100°C/min to 950°C. An optical pyrometer monitored the temperature. At 950°C, a uniaxial pressure of 50 MPa was applied for 15 minutes to complete the sintering process.

4. Results and Discussion

4.1 Yttrium-Doped $BaTiO_3$ for Next-Generation Multilayer Ceramic Capacitors

4.1.1 Structural analysis using XRD

The XRD analysis was conducted to determine the phase purity and crystallinity of yttrium doped barium titanate ($Ba_{1-x}Y_xTiO_3$) at various doping concentrations (x = 0.00, 0.05, 0.125, 0.15, 0.2, and 0.3). The study used XRD spectra between 20 and 90-degree scan angles, and the samples were heated to 950 °C. The results showed that the powdered samples had a perovskite structure, as indicated by the diffraction pattern in Figure 4. The diffraction peaks observed at $2\theta° = 22.23°$, 31.41°, 38.74°, 44.96°, 45.42°, and 50.79° matched with those reported in the previous studies [15], [12]. The XRD analysis revealed that the average diffraction peaks of the samples were consistent with JCPDS card no. 00-005-0626, which indicates a tetragonal formation of $BaTiO_3$ ceramic for all the samples except x = 0.03, which shows a pseudocubic structure. This is likely due to the fact that yttrium is dissolved up to a certain depth in the BT particles [129], which leads to a reduction in tetragonality. A similar outcome was reported by Kim et al., who found that the ferroelectricity of BT decreases significantly when the grain size is below 7μm and the structure changes from tetragonal to pseudocubic [30]. The phase changes observed in the samples are a combination of

tetragonal and cubic phases, which are presented as a pseudocubic phase. The XRD pattern of BT powder shows a pure tetragonal phase, but as the concentration of Y_2O_3 increases, there is a decrease in tetragonality. This result is consistent with our previous studies [14], [31], [32].

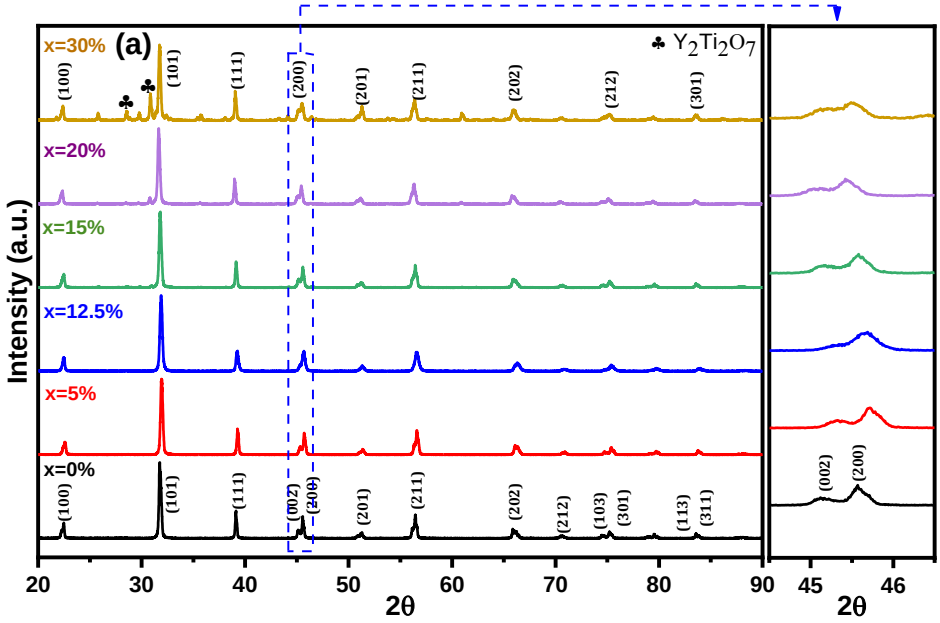

Figure 4. XRD patterns of Y-$BaTiO_3$ ceramics

4.1.2 Surface structure measurement using FESEM

Figure 5(a-c) shows FESEM micrographs of the BT, BY20%, and BY30%T pellets. The FESEM micrographs of the BT sample reveal an assortment of non-uniform grains with some coalescence. The interiors of the fleshy grains are clearly visible in the BT sample. Noticeable changes in the texture of the grains are observed with yttrium doping. It can be observed that each composition exhibits a dense microstructure, which can provide favorable electrical properties and improve the electrical stability of ceramics [32]. Furthermore, the grain size decreases with an increase in yttrium content, accompanied by a transition from surface grains with a porous structure to a nanoporous structure. A closer examination of Figures 5(b) and 5(c) shows that the surface layers of the pellets are covered with a large number of smaller grains, as well as larger grains of various shapes. Interestingly, sharp-edged hexagonal-shaped grains are embedded within the matrix of smaller grains in the A-site Y-doped samples. This structure is less pronounced in the simultaneously and B-site doped materials, where sedimentary growth patterns are observed. The irregular surface morphology in Y-doped samples may be attributed to the interaction between granular surfaces facilitated by the dopant cation.

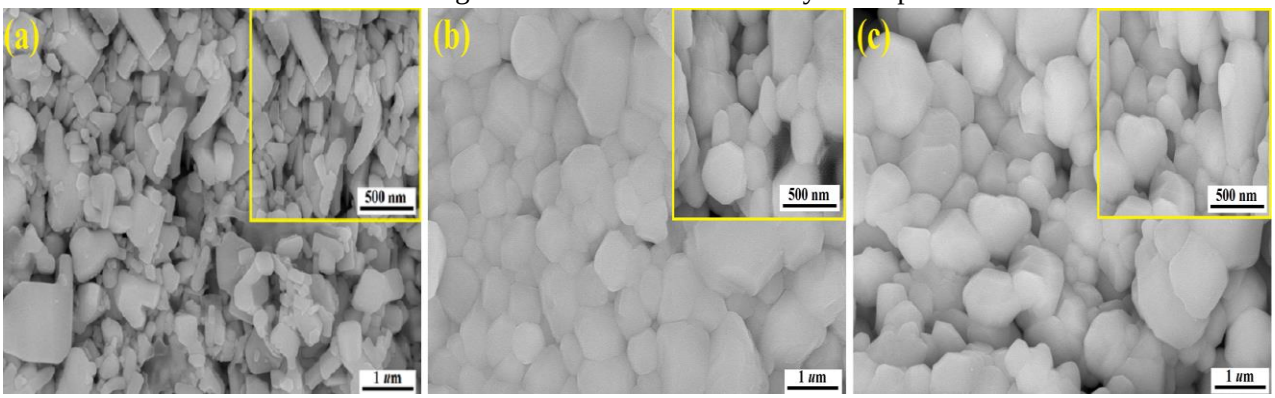

Figure 5. FESEM micrographs of $Ba_{1-x}Y_xTiO_3$ (where a, b, and c are x=0.00, 0.2, and 0.3 respectively)

An energy-dispersive X-ray spectrometer EDAX Octane Elect-Plus was used to check the distribution of individual elements within the grains. The EDS investigations show that the obtained ceramics contain only the elements introduced as substrates, with no other impurities detected in the spectrum. The content of barium and titanium elements slightly differs from the theoretical stoichiometry, whereas the content of yttrium is encumbered by a small uncertainty, which is related to their small participation in the whole mass of the sample, smaller than the threshold of device detection.

The surfaces of the samples were checked in terms of element distribution homogeneity (Figures 6(a), 6(b), and 6(c)). The presence of each element is shown on the mapping in the form of points, where density informs about its concentration. The obtained results indicate that the element distribution is homogeneous in all samples, with some places characterized by lower concentrations due to the microstructural features of the material.

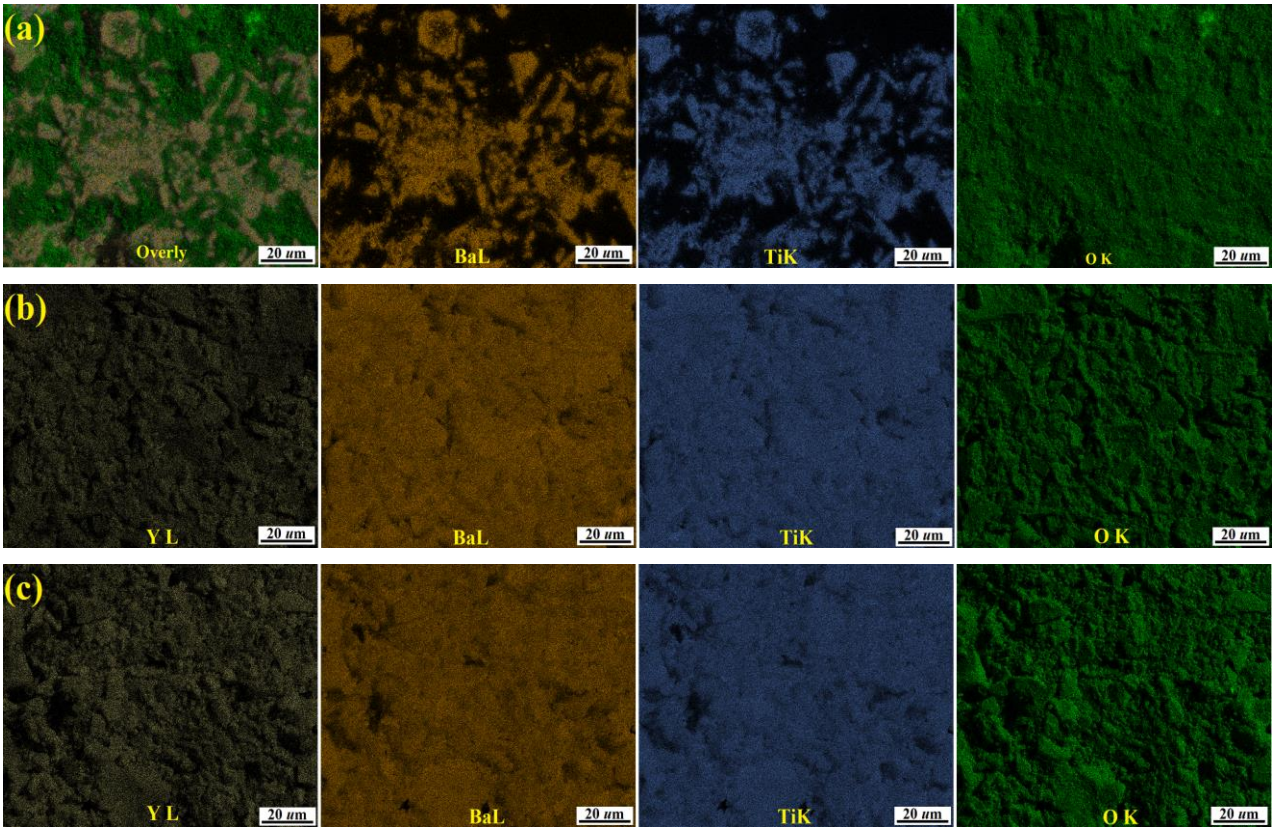

Figure 6. Mapping images for (a) BT, (b)BY20%T, and (c) BY30%T

4.1.3 Optical properties

The crystalline structure of perovskite materials affects their physical and optical properties. UV-Visible absorption spectroscopy (350-800 nm) shows that Y-doped BT ceramics absorb visible photons above 400 nm, peaking at 45% absorption for highly doped samples. This absorption reduces the UV spectra. All Y-doped samples display three distinct peaks in the visible region, with Y occupancy slightly influencing photon absorption.

The optical band gap value, the Tauc functions were used for BYT with the assumption that n=2. As shown in Figure 7, the Eg values of BYxT (x=0, 5, 12.5, 15, 20, and 30%) obtained by extrapolating the linear part to the horizontal axis are in the range of 3.10 to 2.21 eV, which are considerably lower than that of the pure BT (3.10 eV). The band gap reduction of BY30%T (Figure 7(f)) is the most evident, and it's even more significant than those of other photovoltaic perovskite ceramics [20], [21]. The optical behavior of the materials can be explained by the electronic states of the highest energy band

that is occupied by electrons (VBM) and the next highest energy band above the valence band that is unoccupied (CBM) generated by Y^{3+} cation doping. In BT, the VBM is around the O 2p orbital, which has a slight interaction with the Ti 3d and Ba 6p orbitals, whereas the CBM is around the Ti 3d orbital [45]. All these results suggest that the optical properties of BYxT (x=0-30%) ceramics can be regulated and the synthesized ceramics are good candidates for high-performance multilayer ceramic capacitors.

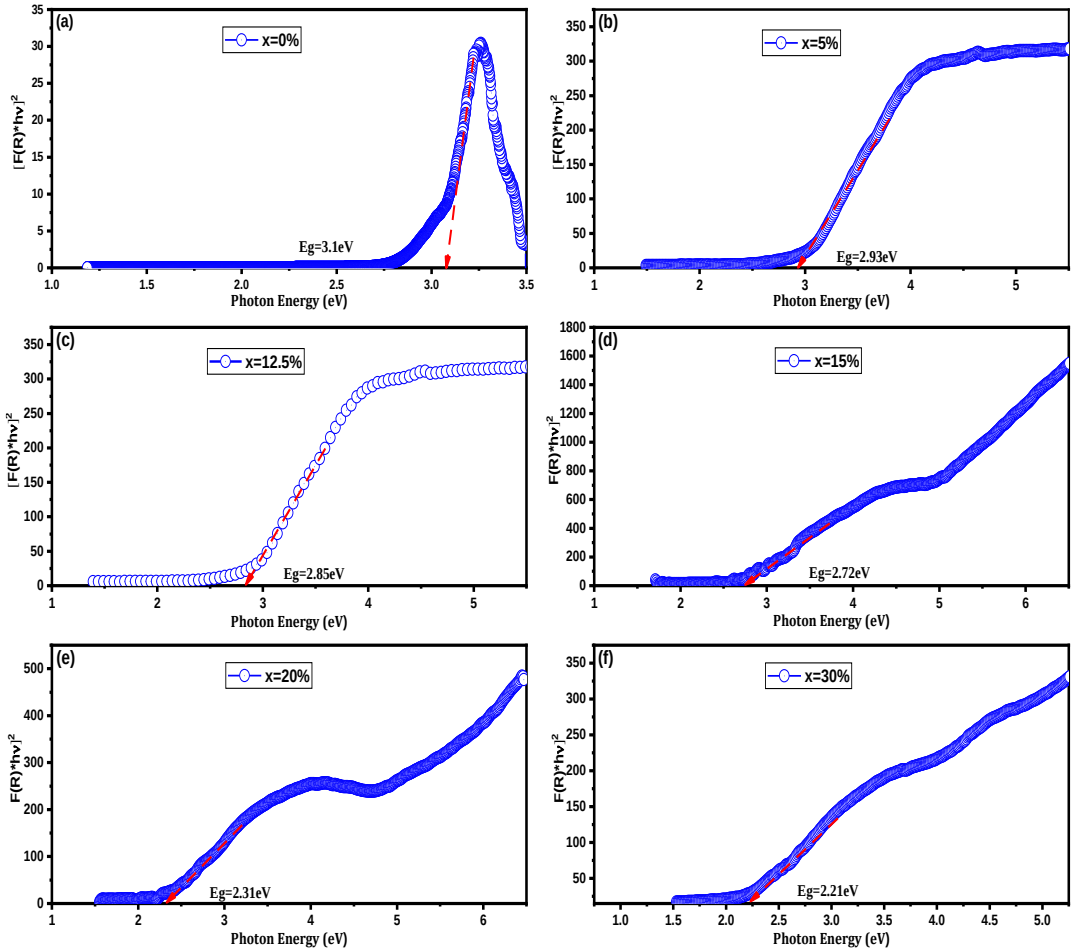

Figure 7. Band gap energy from Tauc plot of (a) BT, (b) BY5%T, (c) BY12.5%T, (d) BY15%T, (e) BY20%T, and (f) BY30%T

4.1.4 Thermal and electrical properties

The thermal and electrical conductivities of $Ba_{1-x}Y_xTiO_3$ ceramic samples (BYxT) were examined as a function of yttrium content at room temperature and 180°C, as illustrated in Figure 8. $BaTiO_3$ has lower thermal and electrical conductivity compared to Y, thus the addition of Y in $BaTiO_3$ system will lead to a percolation behavior. As the concentration of Y increases, the thermal and electrical conductivities follow a power law pattern, as demonstrated in equations (1) and (2) [51],

$$k \propto (V_T - V)^{-q} \quad \text{for } V<V_T \tag{1}$$

$$\sigma \propto (V_E - V)^{-t} \quad \text{for } V<V_E \tag{2}$$

The thermal and electrical conductivities of $Ba_{1-x}Y_xTiO_3$ ceramic samples (BYxT) were studied as a function of yttrium content. Equations (1) and (2) were used to estimate the thermal and electrical conductivities as a function of Y content, and the percolation threshold (V_T and V_E) was calculated. When the Y content is low, the heat conduction is mainly dependent on the vibration of phonons and

the electrons play a minor role. The phonon scattering effect makes it difficult to improve thermal conductivity significantly. As the Y content increases, the Y phase becomes interconnected, allowing electrons to move freely and carry heat, resulting in a percolation behavior. The thermal percolation threshold V_T is 12.5% and the electrical conductivity of the compounds increases sharply when Y content increases from 12.5 to 30 %. The electrical percolation threshold V_E is calculated to be 12.5%. Although V_T is very close to V_E, BYxT samples with 12.5 % of Y content show a high thermal conductivity and relatively low electrical conductivity. The electrical conductivity of all the samples increases with measurement temperature which is typical of semiconducting behavior as shown in Figure 8(b). The sample 30%Y BT has a notably higher electrical conductivity when compared to other samples. Our research aimed to investigate the impact of yttrium doping on the electrical properties of $BaTiO_3$ for use in MLCCs. Since $BaTiO_3$ is naturally insulating, adding Y in atomic percentage improves the electrical conductivity and converts it into an n-type semiconducting material through electron doping. Other dopants have also been shown to improve the electrical conductivity of $BaTiO_3$ in previous studies [39], [38].

The thermal conductivity of all the samples increases with temperature, as shown in Figures 8(a) and 8(b). The sample BY30%T BT has the highest thermal conductivity, which is likely due to the charge compensation of defects in the crystal structure near the Y atoms, which improves the electronic conductivity. Notably, the thermal conductivity of the sample with nanostructured pores (BT sample) is significantly lower compared to the sample BY30%T which has less nano porosity.

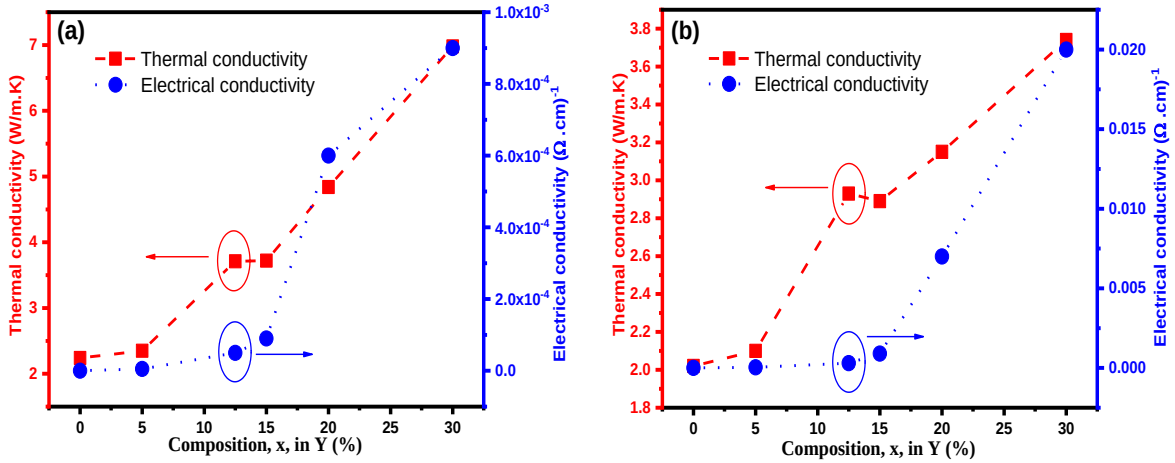

Figure 8. Thermal conductivity and electrical conductivity of BYT as a function of Y content at (a) Room temperature and (b) 180°C

4.2. $Ba_{0.85}Sr_{0.15}TiO_3$/Cu new composites: via sol-gel and spark plasma sintering

4.2.1 Phase analysis using XRD

The XRD patterns tested at room temperature of BST-Cux (x=0, 5, 12.5, 15, 20, 30, and 40%) composites sintered at a low temperature of 950 °C are shown in Figure 9a. All peaks were attributed to either the BST phase or Cu without any impurities being observed, suggesting that no reaction took place between BST and Cu during the SPS sintering process. Furthermore, the diffraction peaks of BST in the composites did not shift, indicating that the copper was not incorporated in the perovskite structure. As expected, the relative diffraction intensities of the Cu reflections compared to the ones of BST increased with the increase of Cu content (Figure 9b). The evolution of the XRD-peaks confirms the successful composition control during sintering. Additionally, the crystal structure of BST-Cu

samples has been proved to be multiphase coexistence of cubic and tetragonal phases at room temperature [181], while the phase of BST as mentioned above is a tetragonal structure.

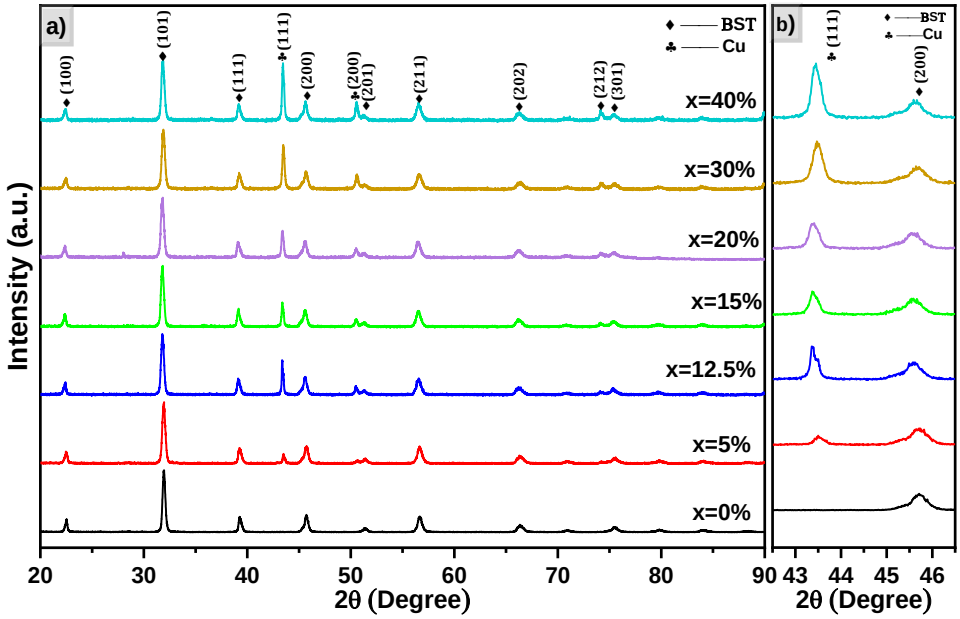

Figure 9. (a) XRD pattern of BST-Cux (x=0-40%) ceramic-metal composites (b) Shifting of the peaks BST (200) and Cu (111)

4.2.2 SEM Investigation

SEM micrographs of BST-Cu composites (0, 5, 12.5, 15, 20, 30, and 40 wt.% Cu) are shown in Figure 10. Grain shapes were irregular and increasing Cu content led to more reactions and intermediate phases. Abnormal grain growth was observed, with pure BST grains at ~3.1µm and BST-Cu grains at 3.1-5.2µm, due to a low eutectic liquid phase between Cu and BST during sintering. Spheroidal Cu particles were seen in the BST matrix, identified by EDS. Increased Cu content caused Cu agglomeration and decreased relative density due to pores. SEM showed decreased porosity with more Cu, consistent with XRD findings. These properties suggest potential for hydroelectric cell applications.

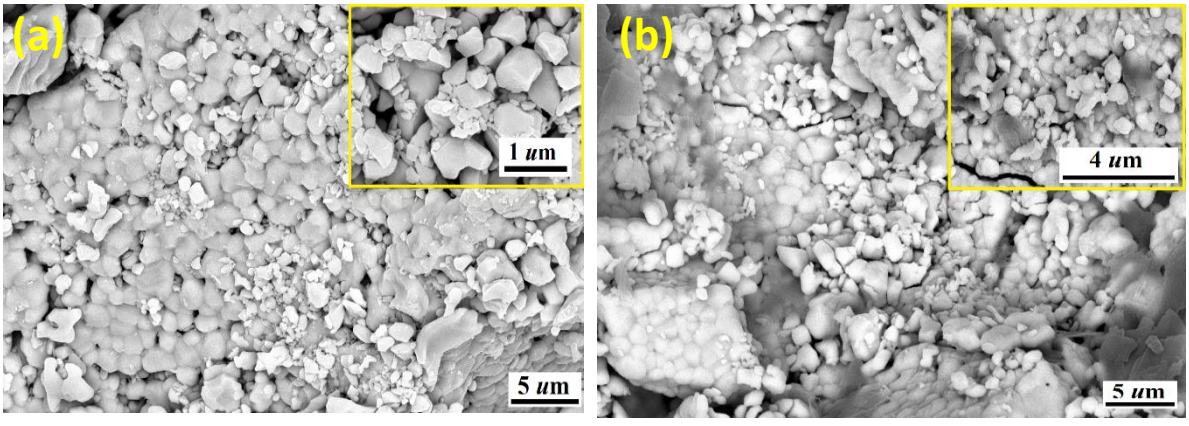

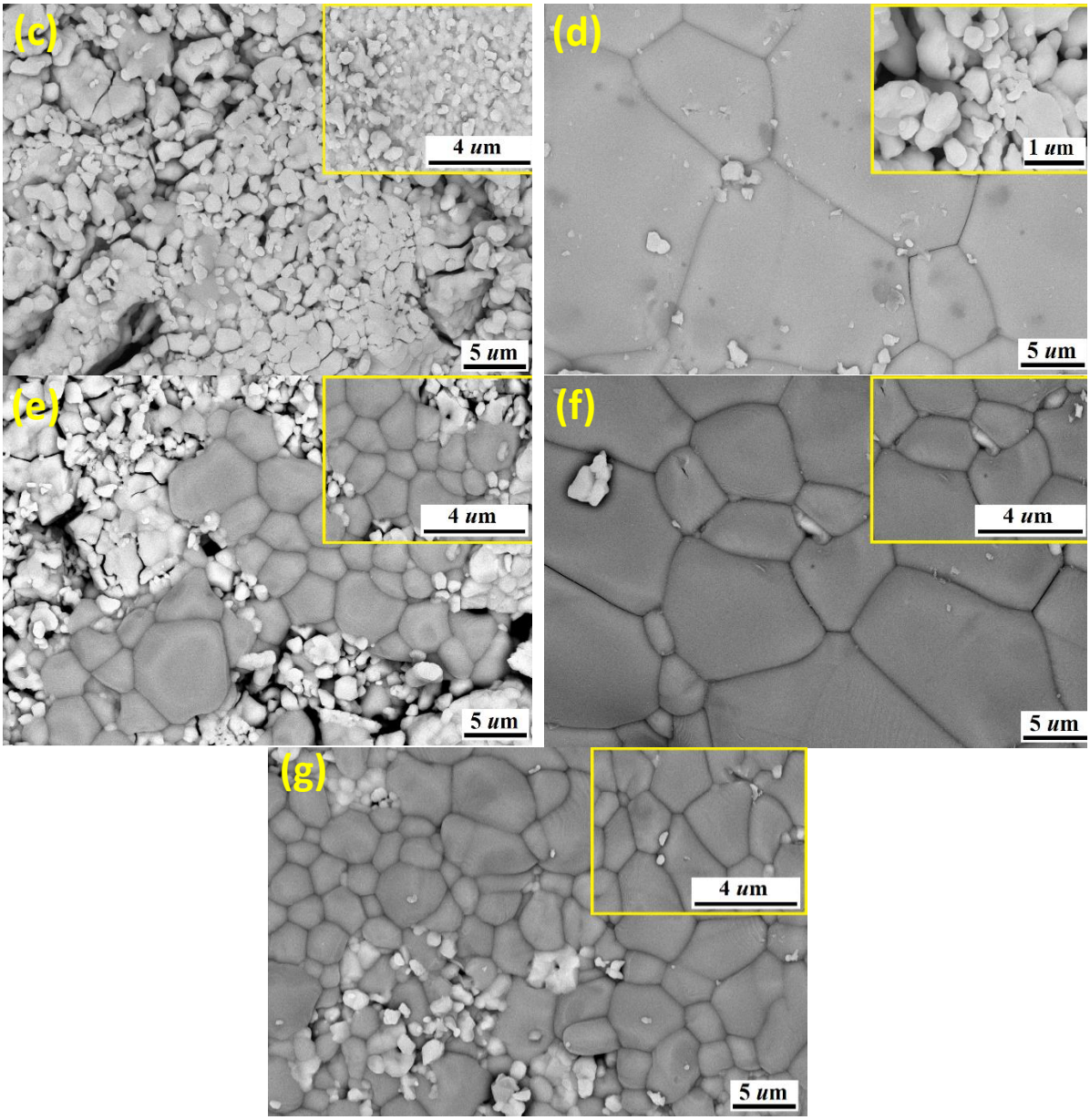

Figure 10. FESEM micrographs of the ceramic samples (a) BST, (b) BST-Cu5%, (c) BST-Cu12.5%, (d) BST-Cu15%, (e) BST-Cu20%, (f) BST-Cu30%, (g) BST-Cu40%

4.2.3 Optical characteristics

The optical band gap energy (E_g) of BST-Cux (x = 0-40%) samples was determined using the Kubelkae-Munk (K–M) method, the latter was used to extract E_g values, as well as the stimulation of the measured diffuse reflectance at a high accuracy [42].

As demonstrated in Figure 11, the Eg values of BST-Cux (x=0, 5, 12.5, 15, 20, 30, and 40%) obtained by extrapolating the linear part to the horizontal axis are in the range of 3.10 and 2.01 eV which are considerably lower than that of the BST (3.10 eV). Among them, the band gap reduction of BST-Cu30% (Figure 11(f)) is the most evident and is even more significant than those of other photovoltaic perovskite ceramics [43], [44].

These optical behaviors can be explained by the newly emerging electronic states of the highest energy band that is occupied by electrons (VBM) and the next highest energy band above the valence band that is unoccupied (CBM) generated by Sr^{2+} cation doping. In BST, the VBM is around the O 2p orbital, which has a slight interaction with the Ti 3d and Ba 6p orbitals, whereas the CBM is around the Ti 3d

orbital [145]. Consequently, all the above-presented results indicate that the optical properties of BST-Cux (x=5, 12.5, 15, 20, 30 and 40%) ceramics can be regulated, demonstrating that the synthesized ceramics are good candidates for high performance multilayer ceramic capacitors.

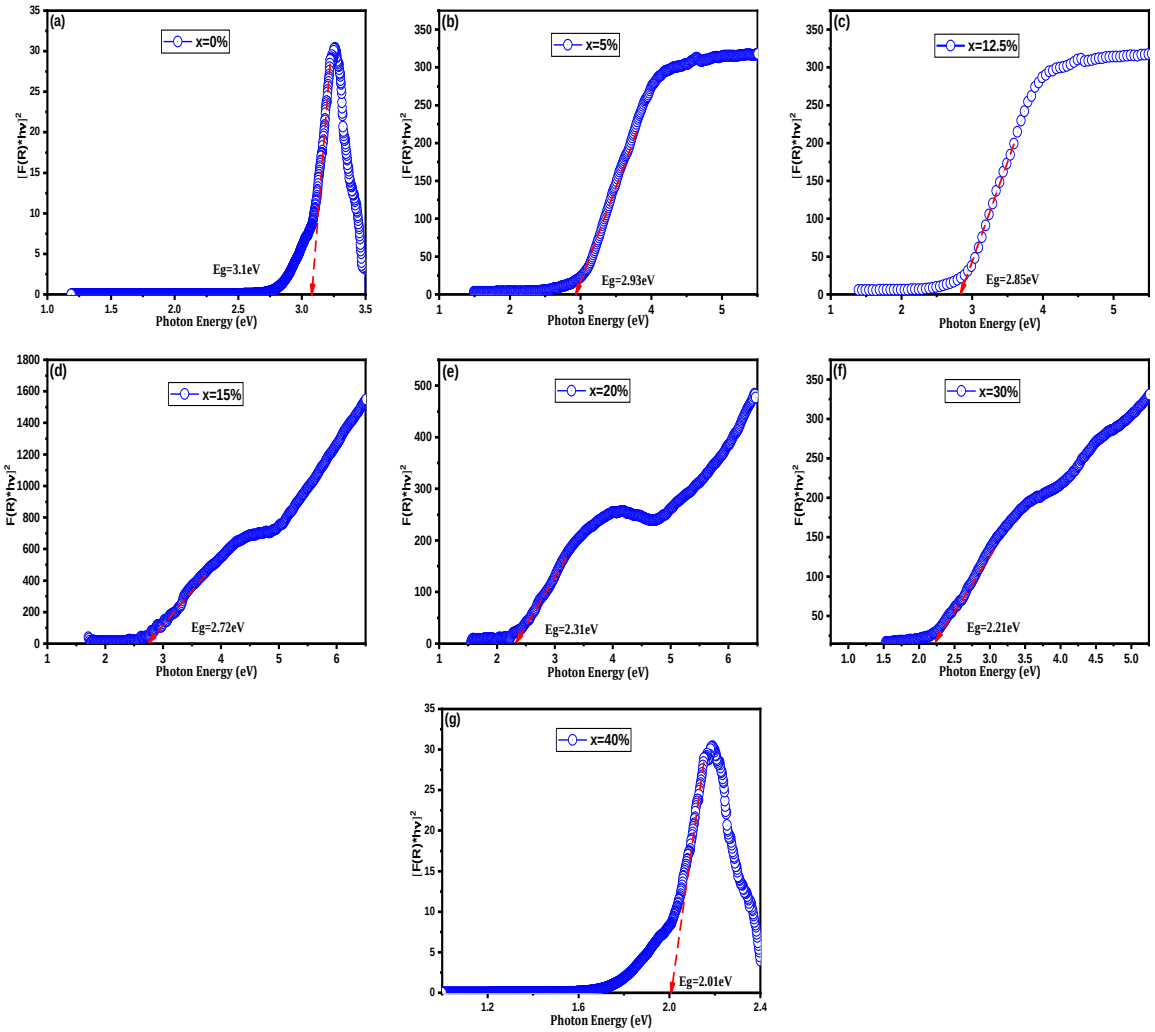

Figure 11. Band gap energy of (a) BST, (b) BST-Cu5%, (c) BST-Cu12.5%, (d) BST-Cu15%, (e) BST-Cu20%, (f) BST-Cu30%, and (g) BST-Cu40%

4.2.4 Electrical conduction mechanism in $BaTiO_3$–Cu composites

The graph in Figure 12 illustrates the change in the real part of AC conductivity (σ′) concerning frequency at room temperature, considering various additions of Cu. The AC conductivity shows a gradual increase with rising Cu concentrations up to 30 wt%, followed by a decline as the Cu content continues to increase. This shift in conductivity is attributed to fluctuations in the concentration of charge carriers within the composites. As the Cu content surpasses a specific threshold (percolation threshold), the concentration of charge carriers decreases due to the emergence of the Cu liquid phase during sintering. This phenomenon aligns with the apparent density variations in the composites with different Cu contents. The percolation threshold for BST-Cux is identified at x = 30 wt%. At lower frequencies, a distinct plateau, more pronounced in samples with higher Cu contents than lower ones, reflects the direct current conductivity (σ_{dc}). Conversely, at higher frequencies, a dispersive region, known as the "universal dielectric response" (UDR), becomes evident. This can be approximately characterized as follows [45]:

$$f_m = \frac{1.8 \times 10^{12}}{\varepsilon\rho} \quad (3)$$

In this context, the dispersive frequency fm is defined as the point at which the transition from the plateau-type region of direct current conductivity σ_{dc} towards the dispersive region occurs. The permittivity (ε) represents the ceramic's ability to permit the flow of electric field at low frequencies, while the resistivity (ρ) indicates the resistance of the ceramic. Observations suggest that as the Cu content increases (resulting in a decrease in resistivity, ρ), there is a corresponding shift in the threshold frequency. This shift denotes the point at which the transition from the plateau-type region of σ_{dc} towards the dispersive region occurs, and it moves towards higher frequency values.

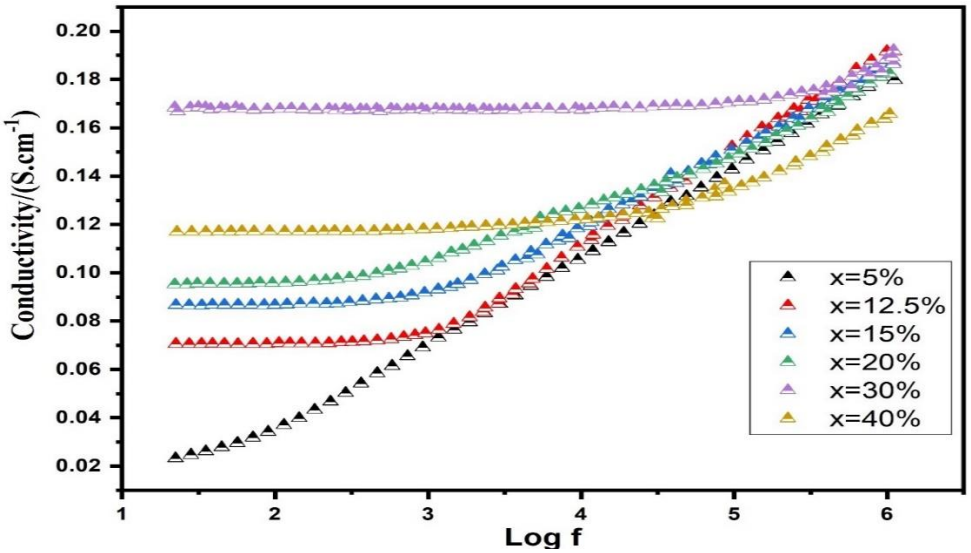

Figure 12. Frequency-Dependent modulation of AC Conductivity (σ′) with varying Copper additions at Room Temperature

Figure 13 illustrates the temperature dependence of conductivity in BST-Cu composites with varying Cu content, focusing on x = 30 wt%. Below the critical temperature (130°C), conductivity increases with temperature, typical of semiconductors, as electrons gain energy to move from the valence band to the conduction band. Above 130°C, conductivity decreases, reflecting the behavior of conducting materials where electron movement becomes more directional. This shift is due to the different conduction mechanisms in semiconductors and conductors. However, at higher temperatures, the electrons experience more intensive scattering by metal atoms or ions, hindering their movement and causing a decrease in metal conductivity. The activation energy for conduction was determined to be 0.18 eV below 83°C and 0.13 eV between 83°C and 130°C. The points of inflection in the temperature-conductivity characteristic at 83°C and 130°C are denoted in Figure 13. It is noteworthy that the activation energy in all samples was significantly smaller than the band gap for intrinsic electronic conduction in BST (≈3.1 eV), indicating the dominance of extrinsic conduction mechanisms associated with defects. Berglund and Braun demonstrated that impurity states, approximately 0.2–0.3 eV below the conduction band, were linked to oxygen vacancies and band conduction[185] . The BST-Cu composites in our study were typically sintered in using spark plasma sintering. As a result, the sintering process under low oxygen partial pressure likely generated a certain amount of oxygen vacancies.

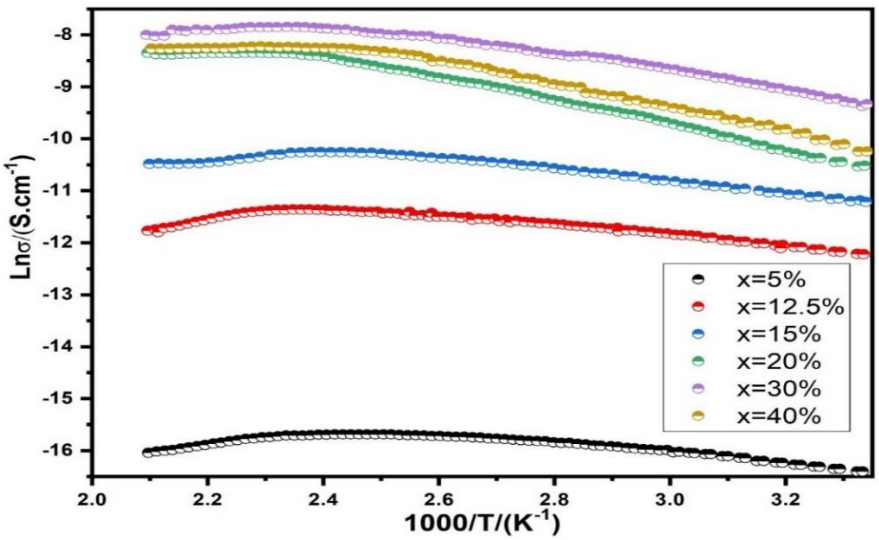

Figure 13. The temperature dependence of the conductivity for different Copper Content.

Figure 14 depicts complex plane plots for impedance, denoted as Z*, in the BST-Cux composites. These plots illustrate the relationship between the imaginary part (Z″) and the real part (Z′). Typically, in the case of a flawless crystal, the resistance (R) and capacitance (C) values are examined using an equivalent circuit consisting of a single parallel RC element. On the complex plane, this RC element manifests as a semicircular arc with intercepts at zero and R on the Z′ axis. Consequently, C, can be determined using the formula ω_{max}RC = 1 where ω_{max} = $2\pi f_{max}$ and fmax and fmax represents the frequency at the maximum point of the arc. For BST-Cu composites, the equivalent circuit is conceptualized as two parallel RC elements connected in series, resulting in the appearance of two arcs on the complex plane.

As depicted in Figure 14, it is evident that the Z″ peak value attributed to grain boundary responses surpasses that of grain responses. Consequently, across all examined samples, R_{gb} is significantly greater than R_g, and the R_{gb} diminishes with escalating Cu content, aligning with the observations in Figures 12 and 13. These outcomes are elucidated through a two-layer model, postulating the existence of conducting grains isolated by poorly conducting grain boundaries.

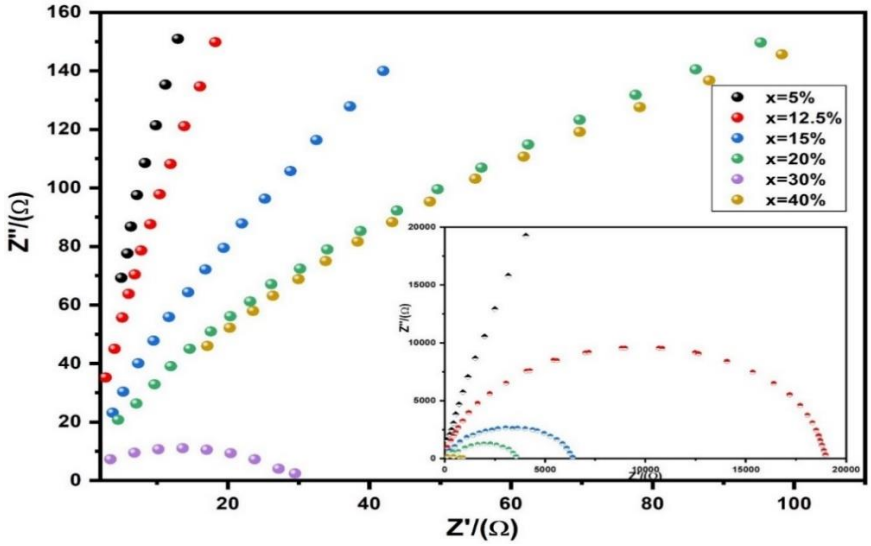

Figure 14. The expanded view of the low frequency and the equivalent circuit of the RC element. The inset represents the impedance complex.

Figure 15 shows the frequency-dependent permittivity of BST-Cu composites at room temperature. For Cu contents of 5, 12.5, and 15 wt%, permittivity shows a subtle frequency dependency from 100 Hz to 1 MHz, similar to pure BST. With Cu at 30 wt%, permittivity peaks at approximately 1.2×10^5 at 1 kHz but declines at low frequencies (around 10^4 Hz) for Cu > 30 wt%, indicating a step decrease where tanδ shows a relaxation peak [18]. This behavior aligns with the Maxwell–Wagner capacitor model, where different phases have distinct conductivity, and charge accumulation at interfaces influences polarization. Conductivity of BST-Cu composites rises with increased Cu content. If Cu acted as an acceptor in the BST lattice, a reduction in conduction electrons would be expected, but the observed behavior suggests otherwise. The differing electrical conduction between BST-Cu and BST-Ni composites likely results from variations in oxygen vacancy concentrations and sintering conditions.

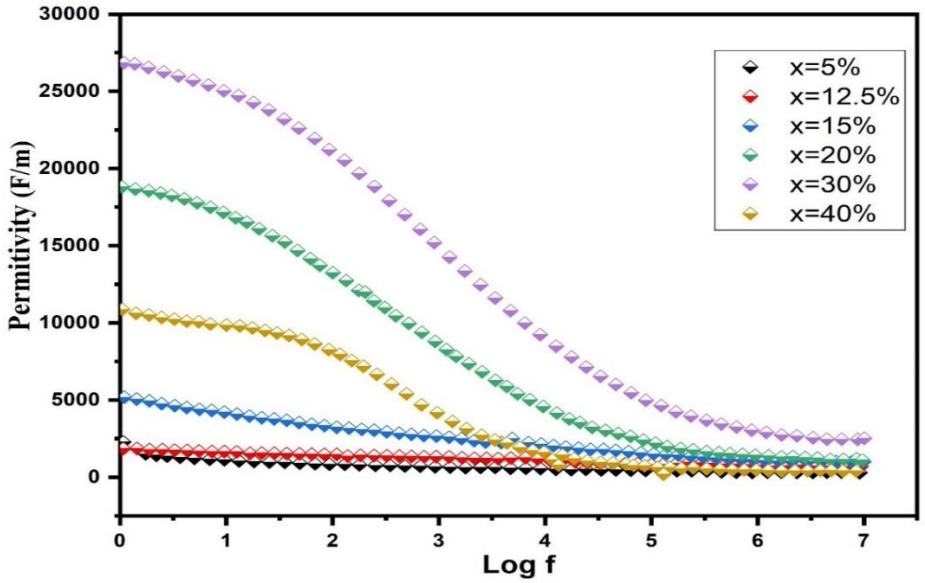

Figure 15. Permittivity of BST-Cu_x (x=5,12.5, 15, 20, 30 and 40%) composites

5. Conclusions

$BaTiO_3$ and various doped ceramics were synthesized via sol-gel. Their structural, optical, thermal, and mechanical properties were detailed. X-ray diffraction and FT-IR confirmed tetragonal and cubic structures. SEM showed flat block particles, and EDS confirmed high purity. Y and Sr dopants altered thermal conductivity by affecting Ti-O bond distances and strengths. UV-vis spectroscopy revealed decreased optical band gaps due to oxygen vacancies and lattice distortions. Compressive strength decreased with Sr and Y doping, linked to grain size and shape. Dense BST-Cu composites (5-40%) were made using spark plasma sintering. AC conductivity increased with Cu content and temperature, shifting from oxygen vacancy migration to band conduction. Conductivity rose below the Curie temperature and declined above 130°C due to different conduction mechanisms. In micro-optical electro-mechanical systems, the studied materials could function as multipurpose, smart materials by fusing their exceptional physical and optical properties.

- The optical band gap energy was found in the semiconducting range of 3.1–2.21 eV. The thermal and electrical conductivity of $BaTiO_3$ has been improved by optimizing the doping of yttrium in weight percentages and causing the samples to become semiconductor materials. The electrical conduction mechanism in doped ceramics could be attributed to the passage of free carrier chargers through a material. The work in this paper is fundamental to the understanding

of the defects associated with the crystal structure and thermoelectric behavior of Y-doped $BaTiO_3$ ceramics and can provide a reference for the application in the MLCC industry.

- The impedance plots revealed higher Z″ peak values at grain boundaries compared to grains, indicating a two-layer model with conducting grains separated by poorly conducting grain boundaries. The grain boundary resistance (R_{gb}) decreased with elevated Cu content.
- The dielectric behavior of BST-Cu composites exhibited variability based on the phase ratio. Remarkably, composites with 30 wt% Cu content achieved a maximum permittivity of $1.0x10^5$ at 1 kHz. Furthermore, these composites displayed elevated permittivity at low frequencies compared to high frequencies, attributed to Maxwell–Wagner polarization.

6. New scientific results

Based on the integrated experimental research studies of pure and doped Barium titanate synthesized using sol-gel method, the following new scientific findings were derived:

1st Claim. Low-temperature preparation of pure and doped barium titanate ceramics using modified sol-gel method.

It was demonstrated that doped barium titanate can be produced at low temperatures using a modified sol-gel method. Drawing from cutting-edge research and insights from prior published works, this innovative process integrates barium acetate trihydrate [$Ba(CH_3CO_2)2{\cdot}3H_2O$] and titanium isopropoxide [$Ti[OCH(CH_3)_2]_4$] as primary precursors, while introducing lactic acid and acetic acid as pivotal stabilizing agents, a strategic evolution inspired by recent investigations into solution chemistry optimization. The process commences with the dissolution of titanium isopropoxide in a precisely calibrated mixture of water and acetic acid, maintaining a delicate equilibrium at 70°C while employing a novel agitation mechanism operating at 300rpm, a nuanced refinement inspired by computational modeling insights into fluid dynamics. This meticulous orchestration yields a stable solution, epitomized by the emergence of a transparent TiO_2 matrix, a characteristic emblematic of optimized nucleation kinetics uncovered through state-of-the-art spectroscopic analyses. Subsequently, the dissolution of barium acetate in distilled water at an elevated temperature of 90°C for a meticulously timed duration of 15 minutes signifies a strategic departure from conventional approaches, a paradigm shift informed by recent breakthroughs in reaction kinetics elucidated through advanced kinetic modeling algorithms. This transformative fusion of precursors sets the stage for gel formation, followed by a judicious drying regimen that exploits recent advances in controlled atmosphere processing, ensuring the preservation of critical structural features. The resultant xerogel undergoes a transformative process within an agate mortar, guided by insights gleaned from advanced particle engineering methodologies, aimed at mitigating powder agglomeration through precise control of mechanical forces. The process culminates in a meticulously orchestrated calcination phase, characterized by the application of temperatures reaching 950°C over a precisely optimized duration of 3 hours, facilitated by recent advancements in thermal profiling techniques that afford unprecedented control overheat transfer phenomena. This harmonious convergence of cutting-edge methodologies and insights from the forefront of materials research heralds a new era in the synthesis of doped barium titanate, offering tantalizing prospects for next-generation electronic devices and energy storage technologies.

2nd Claim. The Effect of Sr Dopants on the Thermal Conductivity of $BaTiO_3$

I have experimentally demonstrated that the thermal conductivity of $BaTiO_3$ samples can be altered by the addition of strontium (Sr) dopant during the low temperature sol-gel method. Increasing the strontium content increases the thermal conductivity from 2.24 (0 m/m% Sr content) to 6.98 $Wm^{-1}K^{-1}$ (30 m/m% Sr content), which is attributed to the strengthened atomic bonds and the altered crystal structural dynamics.

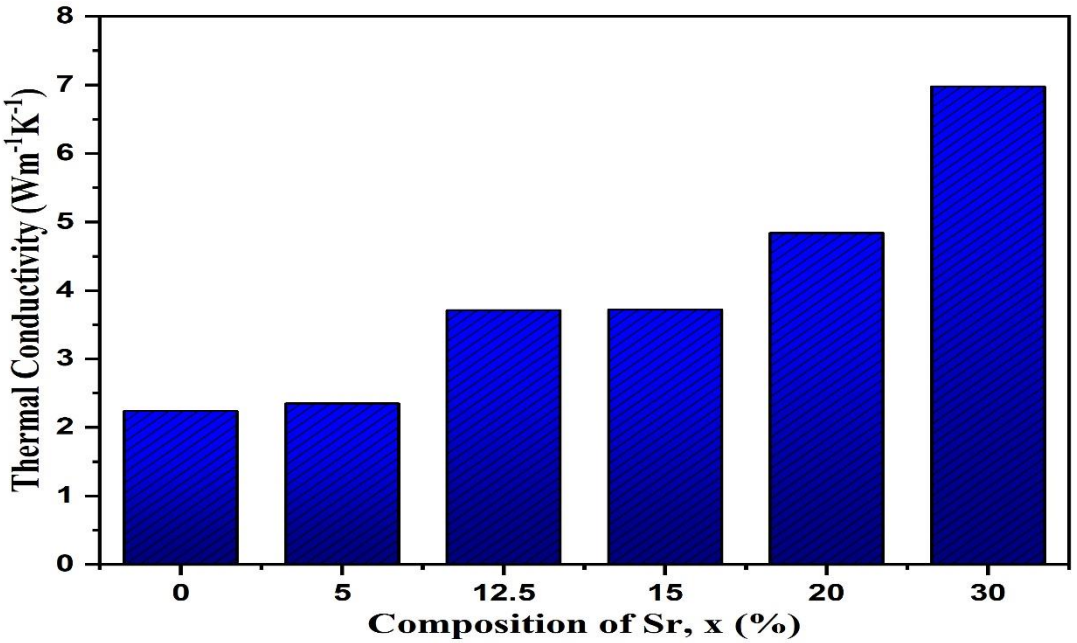

Figure A. The room temperature thermal conductivity of as prepared samples of the BSrxT (x=0, 5, 12.5, 15, 20 and 30%) ceramics

3rd Claim. Band Gap Engineering in Yttrium-Doped Barium Titanate ($BaTiO_3$) for Enhanced Electronic Properties

I have experimentally demonstrated that the addition of Y^{3+} leads to a decrease in the band gap energy of $BaTiO_3$ ceramics prepared by the sol-gel method. The band gap energy of $Ba_{1-x}Y_xTiO_3$, (x=0-0.3) ceramics prepared by doping 0; 5; 12.5; 15; 20 and 30 wt% Y^{3+}, decreases steadily from 3.1eV (Pure $BaTiO_3$) to 2.21eV (30m/m% Yttrium).

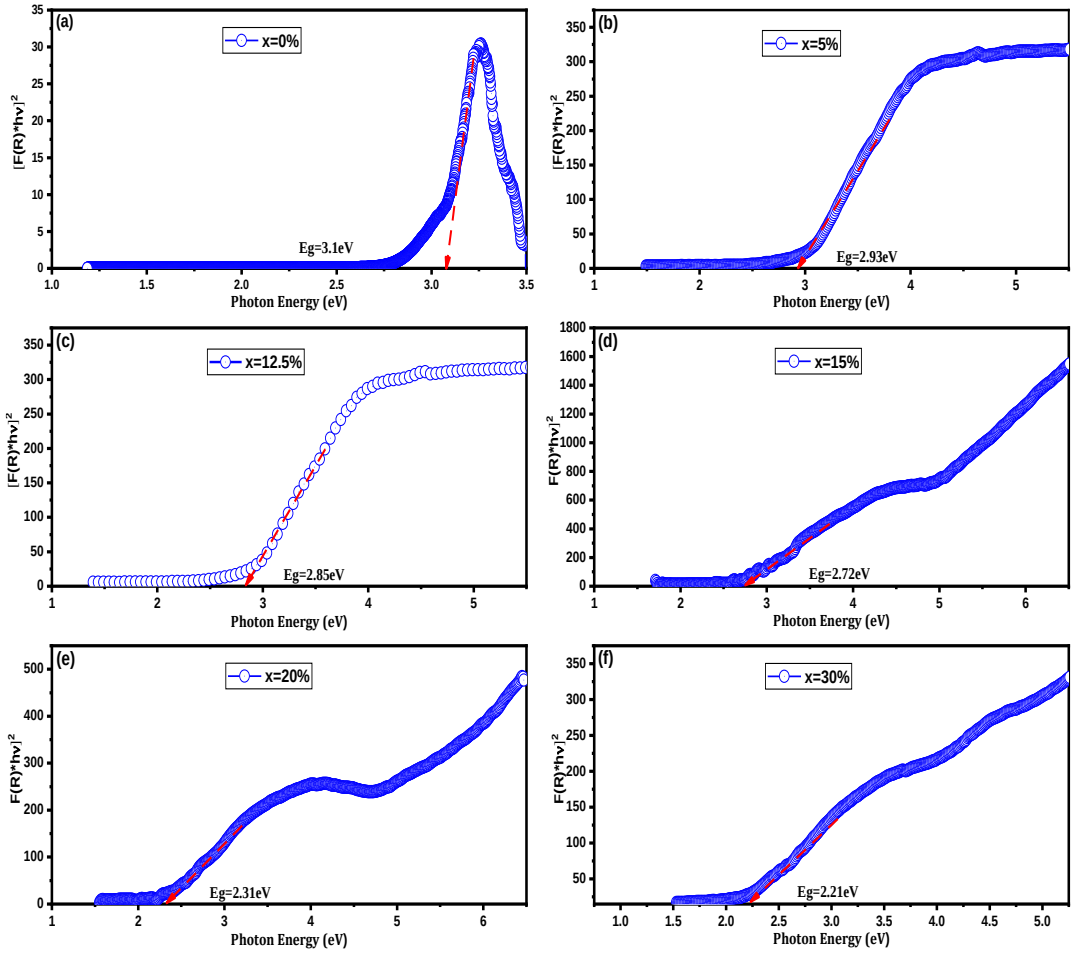

Figure B. Band gap energy from Tauc plot of (a) BT, (b) BY5%T, (c) BY12.5%T, (d) BY15%T, (e) BY20%T, and (f) BY30%T

Table A. Band gap value of $Ba_{1-x}Y_xTiO_3$, (x=0-0.3)

Sample	Band gap value (eV) This work
$Ba_{1-x}Y_xTiO_3$, x=0.00	3.10
$Ba_{1-x}Y_xTiO_3$, x=0.05	2.93
$Ba_{1-x}Y_xTiO_3$, x=0.125	2.85
$Ba_{1-x}Y_xTiO_3$, x=0.15	2.72
$Ba_{1-x}Y_xTiO_3$, x=0.20	2.31
$Ba_{1-x}Y_xTiO_3$, x=0.30	2.21

4th Claim. Effect of Sr and Y Dopants and co-Doping on Mechanical Properties in $BaTiO_3$

I have demonstrated that the 7.5% Sr and Y doping and co-doping ($BaTiO_3$, $B_{1-x}Sr_xTiO_3$, $Ba_{1-x}Y_xTiO_3$, $BaT_{1-x}Y_xO_3$, $Ba_{1-x}Y_xTi_{1-x}Y_xO_3$, and $Ba_{1-x}Sr_xTi_{1-x}Y_xO_3$ (x=0.075) reduces the compressive strength of samples made of the same low temperature sol-gel method $BaTiO_3$ powder by 8.9-17%. The decrease of the strength values of the samples (Fig.C) from 32.91 MPa (pure BaTiO3) to 28.09 MPa ($Ba_{1-x}Sr_xTi_{1-x}Y_xO_3$, x=0.075) and the decrease of the average grain size due to doping from 4.6 µm (pure $BaTiO_3$) to 0.51 µm (BSrTY = $Ba_{1-x}Sr_xTi_{1-x}Y_xO_3$, x=0.075) (Table B) occur in parallel.

Table B. The average Grain size of the compounds

Samples	Grain size (µm)
BT	4.6
BSrT	4.1
BYT	3.7
BTY	3.3
BYTY	0.9
BSrTY	0.5

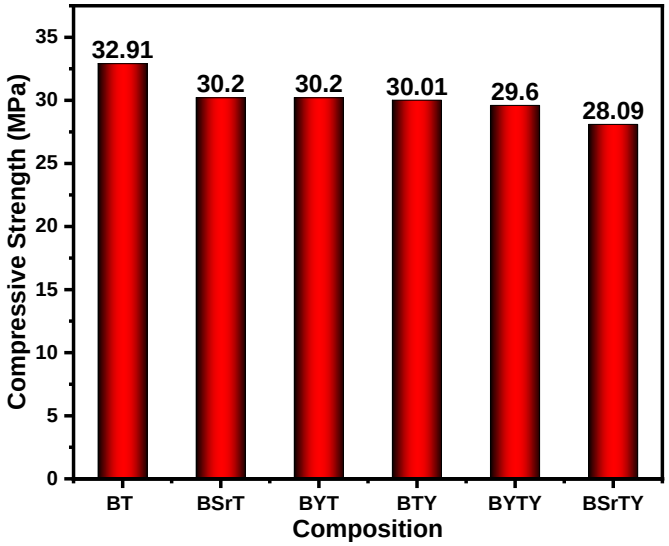

Figure C. Histogram of the compressive strength of the as-prepared BSrT, BYT, BTY, BYTY, and BSrTY samples

5th Claim. Unveiling the Impact of Sr and Y Doping and Co-Doping on the Optical Properties of $BaTiO_3$

The introduction of dual dopants, specifically 7.5% Sr in the Ba-site and 7.5% Y in the Ti-site, demonstrates a novel approach in influencing the conduction band's bottom in ceramic materials. This concurrent doping strategy leads to a significant narrowing of the conduction band, ultimately resulting in a remarkable reduction in the band gap energy. Notably, my research indicates a substantial decrease in the band gap energy from 3.1eV to 2.74eV when employing this dual dopant strategy, compared to materials doped with only one element (either Sr or Y, but not both).

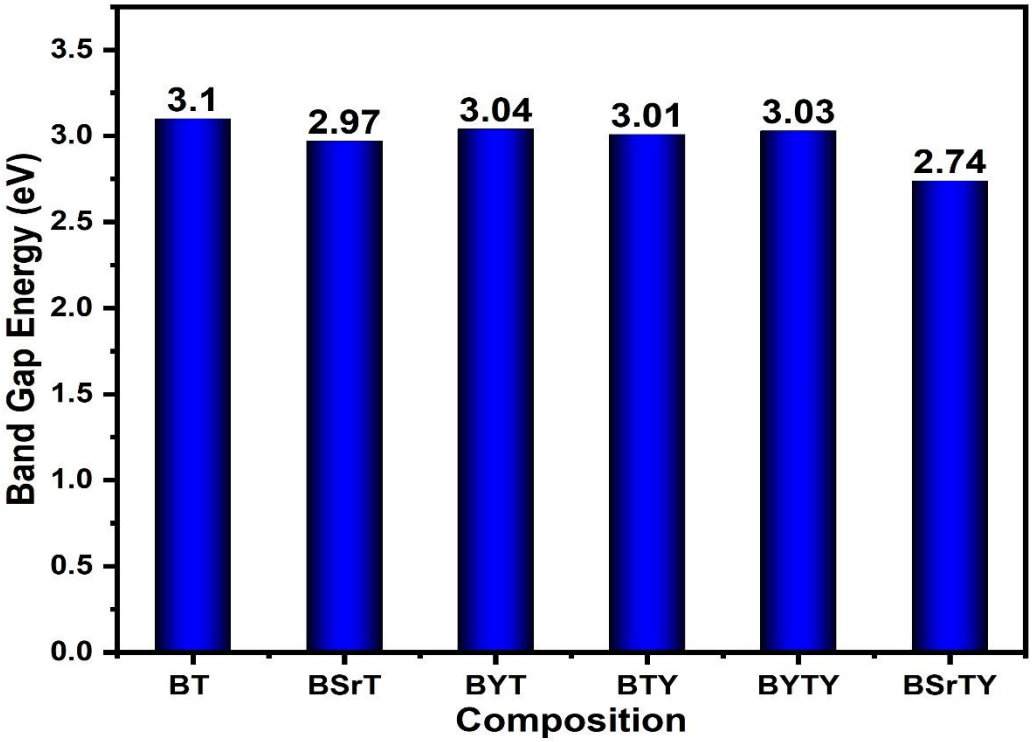

Figure D. Band gap energy of the as-produced samples

6th Claim. Elaboration of new $Ba_{0.85}Sr_{0.15}TiO_3$/Cu composites: via sol-gel and spark plasma sintering

An innovative scientific approach for preparing a new composite, $Ba_{0.85}Sr_{0.15}TiO_3$/Cu, has been established through the integration of the sol-gel method with spark plasma sintering. Barium strontium titanate (BST) powders, synthesized via the sol-gel technique, were combined with high-purity Cu powders (Cu, purity: 99.8%, average particle size: 5µm). The BST powders were initially mixed with Cu content ranging from 0 to 40 wt.% using zirconia balls as grinding media in a ball milling process with ethanol for 12 hours. Subsequently, the slurry was dried, and the resulting mixed powders were extracted. To densify the BST–Cu composite powders, spark plasma sintering (SPS) was employed. During the processing cycle, powder (2–2.6 g) was loaded into a graphite pressure die (inner diameter of 20 mm). The powders, with varying copper content, were heated under vacuum initially up to 600 °C by a preset program within 3 minutes, followed by applying a heating rate of 100 °C/min beyond this temperature until reaching the final sintering temperature (TF = 950 °C). Temperature measurement was conducted using an optical pyrometer focused on the surface of the graphite die, automatically regulating from 600 °C to the final sintering temperature. Upon reaching TF, a uniaxial pressure of 50 MPa was applied, and a dwelling time of 15 minutes was maintained for sintering. Notably, the ceramic samples produced by this novel method exhibited no contamination, demonstrating the ability to achieve high-purity materials even at low temperatures.

7th Claim. Enhanced Electrical and Dielectric Properties of Spark Plasma Sintered BST-Cu Composites

I discovered that the effective engineering and consolidation of dense BST-Cu ceramic composites through spark plasma sintering resulted in a gradual increase in AC conductivity with higher Cu content and temperature. The observed shift in the primary electrical conduction mechanism from oxygen vacancy migration to band conduction involving trapped electrons within oxygen vacancies was notable. Increasing Cu content had a positive impact on electrical conductivity, with a rising trend below the Curie temperature (Tc) and a decline above 130°C. This temperature-dependent behavior was linked to differences in electrical conduction mechanisms between semiconductors and conductors.

Impedance plots revealed higher Z″ peak values at grain boundaries compared to grains, indicating a two-layer model with conducting grains separated by poorly conducting grain boundaries. The grain boundary resistance (R_{gb}) decreased with increased Cu content.
The dielectric behavior of BST-Cu composites displayed variability based on the phase ratio. Remarkably, composites with 30 wt% Cu content achieved a maximum permittivity of $1.0x10^5$ at 1 kHz. Additionally, these composites exhibited heightened permittivity at low frequencies compared to high frequencies, attributed to Maxwell–Wagner polarization.

Publications

Articles related to the dissertation:

1. Mohammed Tihtih, Jamal Eldin FM Ibrahim, Mohamed A. Basyooni, Redouane En-nadir, Walid Belaid, Irina Hussainova and István Kocserha, "Development of Yttrium-Doped BaTiO3 for Next-Generation Multilayer Ceramic Capacitors." *ACS Omega* (2023): *IF (4.10) Q1*
2. Mohammed Tihtih, Jamal Eldin FM Ibrahim, Mohamed A Basyooni, Redouane En-Nadir, Irina Hussainova, Istvan Kocserha, "Functionality and Activity of Sol–Gel-Prepared Co and Fe co-Doped Lead-Free BTO for Thermo-Optical Applications." *ACS Omega* (2023): *IF (4.10) Q1*
3. Mohammed Tihtih, Jamal Eldin FM Ibrahim, Mohamed A Basyooni, Emese Kurovics, Walid Belaid, Irina Hussainova, István Kocserha, "Role of A-site (Sr), B-site (Y), and A, B sites (Sr, Y) substitution in lead-free BaTiO3 ceramic compounds: Structural, optical, microstructure, mechanical, and thermal conductivity properties." *Ceramics International* (2023): *IF (5.2) Q1*
4. Mohammed Tihtih, Jamal Eldin F M Ibrahim, Mohamed A Basyooni, Walid Belaid, László A Gömze, István Kocserha, "Structural, optical, and electronic properties of barium titanate: experiment characterisation and first-principles study." *Materials Technology* (2023): *IF (4.2) Q1*
5. Mohammed Tihtih, Jamal Eldin F M Ibrahim, Mohamed A Basyooni, Walid Belaid, László A Gömze, István Kocserha, "Structural, optical, and electronic properties of barium titanate: experiment characterisation and first-principles study." *Materials Technology* (2023): *IF (4.2) Q1*
6. Mohammed Tihtih, Jamal Eldin FM Ibrahim, Mohamed A. Basyooni, Redouane En-nadir, Walid Belaid, Mohamed M. Abdelfattah, Irina Hussainova, Gábor Pszota and István Kocserha, "Enhanced optical and thermal conductivity properties of barium titanate ceramic via strontium doping for thermo-optical applications." *Optical and Quantum Electronics* (2023): *IF (3.0) Q2*
7. Mohammed Tihtih, Jamal Eldin FM Ibrahim, Emese Kurovics, and László A. Gömze. "Synthesis of $Ba_{1-x}SrxTiO_3$ (x= 0–0.3) ceramic powders via sol-gel method: structural, microstructure, thermal conductivity, and compressive strength properties." *Crystal Research and Technology* 57, no. 1 (2022): 2100106. *IF (1.639) Q2*
8. Mohammed Tihtih, Jamal Eldin FM Ibrahim, Emese Kurovics, and László A. Gömze. "Study of the structure, microstructure and temperature dependent thermal conductivity properties of $SrTiO_3$: via Y^{3+} substitution." In *Journal of Nano Research*, vol. 69, pp. 33-42. Trans Tech Publications Ltd, 2021. *IF (3.06) Q3*
9. Mohammed Tihtih, Jamal Eldin FM Ibrahim, Emese Kurovics, and Mohamed Abdelfattah. "Study on the effect of Bi dopant on the structural and optical properties of $BaTiO_3$ nanoceramics synthesized via sol-gel method." In *Journal of Physics: Conference Series*, vol. 1527, no. 1, p. 012043. IOP Publishing, 2020. *IF (0.55) Q3*
10. Mohammed Tihtih, Aleksei V. Ponaryadov, Jamal Eldin FM Ibrahim, Emese Kurovics, Elena L. Kotova, and László A. Gömze. "Effect of temperature on the structural properties of barium titanate nanopowders synthesis via sol-gel process." *Epitoanyag-Journal of Silicate Based & Composite Materials* 72, no. 5 (2020). *IF (1.079)*
11. Mohammed Tihtih, Karoum Limame, Yahya Ababou, Salaheddine Sayouri, and Jamal Eldin FM Ibrahim. "Sol-gel synthesis and structural characterization of Fe doped barium titanate nanoceramics." *Építöanyag* 6 (2019): 190-193. *IF (1.079)*

Other publications:

1. Redouane En-nadir, Haddou El Ghazi, Mohammed Tihtih, Shrouk E. Zaki, Walid Belaid, Ibrahim Maouhoubi, Izeddine Zorkani.. " Exploring the electronic properties of shallow donor impurities in modified ∩-shaped potential: effects of applied electric field, parabolicity, compositions, and thickness." *The European Physical Journal B* 96(6):78 (2024). *IF (1.6) Q2*
2. Redouane En-Nadir, Mohamed A Basyooni-M Kabatas, Mohammed Tihtih, Haddou El Ghazi. " Innovative sustainable ceramic Bricks: Linear and nonlinear optical absorption coefficients in

InGaN/GaN quantum wells: Interplay between intense laser field and higher-order anharmonic potentials." *Heliyon* (2023). *IF (4.1) Q1*

3. Mohamed A Basyooni, Mohamed Achehboune, Issam Boukhoubza, AEH Gaballah, Mohammed Tihtih, Walid Belaid, Redouane En-nadir, Issam Derkaoui, Ahmed M Abdelbar, Shrouk E Zaki, Şule Ateş, Yasin Ramazan Eker. " Impact of thickness on optoelectronic properties of α-MoO3 film photodetectors: Integrating first-principles calculations with experimental analysis." *Physica B: Condensed Matter* (2023). *IF (2.8) Q2*
4. Jamal Eldin FM Ibrahim, Emese Kurovics, Mohammed Tihtih, Mohamed A Basyooni, István Kocserha. "Reaction synthesis of porous nano-structured mullite ceramic composites from alumina and zeolite-poor rock with enhanced strength and low thermal conductivity." *Results in Engineering* (2023). *IF (5.00) Q1*
5. Redouane En-Nadir, Mohamed A Basyooni-M. Kabatas, Mohammed Tihtih, Walid Belaid, Ilyass Ez-Zejjari, El Ghmari Majda, Haddou El Ghazi, Ahmed Sali, Izeddine Zorkani. " Enhancing Emission via Radiative Lifetime Manipulation in Ultrathin InGaN/GaN Quantum Wells: The Effects of Simultaneous Electric and Magnetic Fields, Thickness, and Impurity." *Nanomaterials* (2023). *IF (5.3) Q1*
6. Mohamed A Basyooni, Mohammed Tihtih, Shrouk E Zaki, Yasin Ramazan Eker. " High-Performance Negative Self-Powered α-MoO3/Ir/α-MoO3 Photodetectors: Probing the Influence of Coulomb Deep Traps." *ACS Applied Electronic Materials* (2023). *IF (7.2) Q1*
7. Redouane En-nadir, Haddou El-ghazi, Liviu Leontie, Mohammed Tihtih, Shrouk E Zaki, Walid Belaid, Aurelian Carlescu, Izeddine Zorkani. " Tailoring optoelectronic properties of InGaN-based quantum wells through electric field, indium content, and confinement shape: A theoretical investigation." *Physica B: Condensed Matter* (2023). *IF (2.8) Q2*
8. Redouane En-nadir, Haddou El-ghazi, Mohammed Tihtih, Walid Belaid, Shrouk E Zaki, Ibrahim Maouhoubi, Izeddine Zorkani. " Analyzing the combined influences of external electric field, impurity-location, in-content, and QW's number on donor-impurity binding energy in multiple quantum wells with finite squared potential." *Optical and Quantum Electronics* (2023). *IF (3.0) Q2*
9. Jamal Eldin FM Ibrahim, Mohammed Tihtih, Ethem İlhan Şahin, Mohamed A Basyooni, István Kocserha. " Sustainable Zeolitic Tuff Incorporating Tea Waste Fired Ceramic Bricks: Development and Investigation." *Case Studies in Construction Materials* (2023). *IF (6.2) Q1*
10. Redouane En-nadir, Haddou El Ghazi, Mohammed Tihtih, Shrouk E Zaki, Walid Belaid, Ibrahim Maouhoubi, Izeddine Zorkani. " Exploring the electronic properties of shallow donor impurities in modified∩-shaped potential: effects of applied electric field, parabolicity, compositions, and thickness." *The European Physical Journal B* (2023). *IF (1.6) Q2*
11. Mohamed A Basyooni, Amina Houimi, Mohammed Tihtih, Shrouk E Zaki, Issam Boukhoubza, Walid Belaid, Redouane En-nadir, Jamal Eldin FM Ibrahim, GF Attia. " Boosting the efficiency of Cu2ZnSnS4 solar cells with VO2 phase transition photonic crystal." *Optical Materials* (2023). *IF (3.9) Q2*
12. Mohamed A Basyooni, AEH Gaballah, Mohammed Tihtih, Issam Derkaoui, Shrouk E Zaki, Yasin Ramazan Eker, Şule Ateş. " Thermionic Emission of Atomic Layer Deposited MoO3/Si UV Photodetectors." *Materials* (2023). *IF (3.4) Q2*
13. Walid Belaid, Haddou El Ghazi, Shrouk E Zaki, Mohamed A Basyooni, Mohammed Tihtih, Redouane Ennadir, Hamdi Şükür Kılıç, Izeddine Zorkani, Anouar Jorio. " A theoretical study of the effects of electric field, hydrostatic pressure, and temperature on photoionization cross-section of a donor impurity in (Al, Ga)N/AlN double triangular quantum wells." *Physica Scripta* (2023). *IF (2.9) Q2*
14. Redouane En-nadir, Haddou El-ghazi, Walid Belaid, Mohammed Tihtih, Hassan Abboudi, Ibrahim Maouhoubi, Anouar Jorio, Izeddine Zorkani. " Intrasubband-related linear and nonlinear optical absorption in single, double and triple QW: the compositions, temperature and QW's number effects." *Philosophical Magazine* (2023). *IF (1.86) Q2*
15. Jamal Eldin FM Ibrahim, Mohammed Tihtih, Emese Kurovics, Ethem İlhan Şahin, László A Gömze, István Kocserha. " Glass-ceramic foams produced from zeolite-poor rock (Tokaj)." *Pollack Periodica* (2023). *IF (0.94) Q3*
16. Mohamed A Basyooni, Mohammed Tihtih, Issam Boukhoubza, Jamal Eldin FM Ibrahim, Redouane En-nadir, Ahmed M Abdelbar, Khalid Rahmani, Shrouk E Zaki, Şule Ateş, Yasin Ramazan Eker. "

Iridium/Silicon Ultrathin Film for Ultraviolet Photodetection: Harnessing Hot Plasmonic Effects." *physica status solidi (RRL)–Rapid Research Letters* (2023). *IF (2.77) Q2*

17. Shrouk E Zaki, Mohamed A Basyooni, Walid Belaid, Mohammed Tihtih, Jamal Eldin FM Ibrahim, GF Attia. " Terahertz resonance frequency through ethylene glycol phononic multichannel sensing via 2D MoS2/PtSe2 structure." *Materials Chemistry and Physics* (2022). *IF (4.6) Q2*
18. Shrouk E Zaki, Mohamed A Basyooni, Mohammed Tihtih, Walid Belaid, Jamal Eldin FM Ibrahim, Mohamed Mostafa Abdelfattah, Amina Houimi, AM Abdelaziz. " Tin diselenide/zirconium disulfide terahertz acoustic multi-layer superlattice for liquid sensing applications of acetonitrile; reconsidering Voigt-Reuss-Hill schemes." *Results in Physics* (2022). *IF (5.3) Q1*
19. Jamal Eldin FM Ibrahim, Mohammed Tihtih, Emese Kurovics, László A. Gömze and István Kocserha. " Innovative glass-ceramic foams prepared by alkali activation and reactive sintering of zeolite-poor rock and sawdust for thermal insulation." *Journal of Building Engineering* (2022): *IF (7.144) D1*
20. Mohamed A Basyooni, Shrouk E Zaki, Nada Alfryyan, Mohammed Tihtih, Yasin Ramazan Eker, Gamal F Attia, Mücahit Yılmaz, Şule Ateş, Mohamed Shaban. " Nanostructured MoS2 and WS2 Photoresponses under Gas Stimuli." *Nanomaterials* (2022). *IF (5.3) Q1*
21. Al-Saudi Sarah Kareem Mohammed, Emese Kurovics, Jamal-Eldin FM Ibrahim, Mohammed Tihtih, Andrea Simon, Róbert Géber. " Preparation of an Aluminum Titania/Mullite Composite from the Raw Materials Alumina, Titania and Silica Fume." *Revue des Composites et des Materiaux Avances* (2022). *IF (1.02) Q3*
22. Jamal Eldin FM Ibrahim, Emese Kurovics, Mohammed Tihtih, and László A. Gömze and István Kocserha. "Synthesis and characterization of alkali-activated zeolite-poor rocks." In Journal of Physics: Conference Series, vol. 2315, no. 1, p. 012020. IOP Publishing, 2022.
23. M Abdelfattah, R Géber, M Tihtih, I Kocserha. " Enhancement the properties of lightweight concrete mortars by some additive materials." In Journal of Physics: Conference Series, 2315 (1), 012005. IOP Publishing, 2022.
24. Mohamed A Basyooni, Shrouk E Zaki, Mohammed Tihtih, Yasin Ramazan Eker, Şule Ateş. " Photonic band gap engineering in (VO2) n/(WSe2) n photonic superlattice for versatile near-and mid-infrared phase transition applications." *Journal of Physics: Condensed Matter* (2022). *IF (2.7) Q2*
25. Emese Kurovics, Jamal-Eldin FM Ibrahim, Mohammed Tihtih, Emese Sebe. " Phase composition and microstructure of ceramics made from kaolin mineral, alumina, and corn starch." *Epitoanyag-Journal of Silicate Based & Composite Materials* 72, no. 5 (2022). *IF (1.079)*
26. Jamal Eldin FM Ibrahim, Olga B. Kotova, Shiyong Sun, Emese Kurovics, Mohammed Tihtih, and László A. Gömze. "Preparation of innovative eco-efficient composite bricks based on zeolite-poor rock and Hen's eggshell." *Journal of Building Engineering* 45 (2022): 103491. *IF (7.144) D1*
27. Jamal Eldin FM Ibrahim, Mohammed Tihtih, Mohamed A Basyooni, István Kocserha. " Innovative sustainable ceramic Bricks: Exploring the synergy of natural zeolite tuff and aluminum dross." *Construction and Building Materials* 297 (2021): 123715. *IF (6.14) D1*
28. Jamal Eldin FM Ibrahim, Afanasy S. Apkarian, Mohammed Tihtih, Sergei N. Kulkov, and László A. Gömze. "In-situ carbonization of natural zeolite-alumina composite materials incorporated sawdust." *Epitoanyag-Journal of Silicate Based & Composite Materials* 73, no. 4 (2021). *IF (1.079)*
29. Jamal Eldin FM Ibrahim, Emese Kurovics, Mohammed Tihtih, and László A. Gömze. "Ceramic bricks with enhanced thermal insulation produced from natural zeolite." *Pollack Periodica* 16, no. 3 (2021): 101-107. *IF (0.87) Q3*
30. Jamal Eldin FM Ibrahim, Mohammed Tihtih, and László A. Gömze. "Environmentally-friendly ceramic bricks made from zeolite-poor rock and sawdust." *Construction and Building Materials* 297 (2021): 123715. *IF (6.14) D1*
31. Irina N Sevostianova, TATIANA YU SABLINA, Sergei N Kulkov, Mohammed Tihtih, LÁSZLÓ A GÖMZE. " Stress-strain behavior of high porous zirconia ceramic." *Epitoanyag-Journal of Silicate Based & Composite Materials* (2021). *IF (1.079)*
32. Jamal Eldin FM Ibrahim, Ayhan Mergen, Umut Parlak, Emese Kurovics, Mohammed Tihtih, and László A. Gömze. "Synthesis and characterization of iron-doped $GdMnO_3$ multiferroic ceramics." *Építöanyag* (Online) 1 (2021): 24-27. *IF (1.079)*

33. Emese Kurovics, Olga B. Kotova, Jamal Eldin FM Ibrahim, Mohammed Tihtih, Shiyong Sun, Péter Pala, and László A. Gomze. "Characterization of phase transformation and thermal behavior of Sedlecky Kaolin." *Építöanyag* (Online) 4 (2020): 144-147. *IF (1.079)*
34. Aleksei V Ponaryadov, Olga B Kotova, Mohammed Tihtih, Shiyong Sun. " Natural titanium dioxide nanotubes." *Építöanyag* (Online) 4 (2020). *IF (1.079)*
35. Jamal Eldin FM Ibrahim, Dmitry A. Shushkov, Emese Kurovics, Mohammed Tihtih, Olga B. Kotova, Péter Pala, and László A. Gömze. "Effect of composition and sintering temperature on thermal properties of zeolite-alumina composite materials." *Epitoanyag-Journal of Silicate Based & Composite Materials* 72, no. 4 (2020). *IF (1.079)*
36. Emese Kurovics, Jamal Eldin FM Ibrahim, Mohammed Tihtih, Bella Udvardi, Kanokon Nuilek, & László A. Gömze. (2020, April). Examination of mullite ceramic specimens made by conventional casting method from kaolin and sawdust. In *Journal of Physics: Conference Series* (Vol. 1527, No. 1, p. 012034). IOP Publishing. *IF (0.55) Q3*
37. Jamal Eldin FM Ibrahim, Kurovics, M. Tihtih, P. Somdee, A. G. Gerezgiher, K. Nuilek, E. E. Khine, and M. Sassi. "Preparation and Investigation of Alumina-Zeolite Composite Materials." In *Journal of Physics: Conference Series*, vol. 1527, no. 1, p. 012029. IOP Publishing, 2020. *IF (0.55) Q3*
38. M Abdelfattah, I Kocserha, R Géber, M Tihtih, F Móricz. " Evaluating the properties and mineral phases of the expanded clay aggregates with the bentonite additive material." In *Journal of Physics: Conference Series*. IOP Publishing, 2020. *IF (0.55) Q3*

Books

Mohamed A Basyooni, Shrouk E Zaki, Mohammed Tihtih, Issam Boukhoubza, Redouane En-nadir, GF Attia. "Fundamentals and Classifications of CO2 Sensors." *Handbook of Nanosensors: Materials and Technological Applications* (2023).

References

[1] T. Zaman, M. K. Islam, M. A. Rahman, A. Hussain, M. A. Matin, and M. S. Rahman, 'Mono and co-substitution of Sr 2+ and Ca 2+ on the structural, electrical and optical properties of barium titanate ceramics', *Ceram Int*, vol. 45, no. 8, pp. 10154–10162, Jun. 2019, doi: 10.1016/j.ceramint.2019.02.064.

[2] Y. Slimani *et al.*, 'Study on the addition of SiO2 nanowires to BaTiO3: Structure, morphology, electrical and dielectric properties', *Journal of Physics and Chemistry of Solids*, vol. 156, p. 110183, Sep. 2021, doi: 10.1016/J.JPCS.2021.110183.

[3] C. Zhao *et al.*, 'Practical High Piezoelectricity in Barium Titanate Ceramics Utilizing Multiphase Convergence with Broad Structural Flexibility', *J Am Chem Soc*, vol. 140, no. 45, pp. 15252–15260, Nov. 2018, doi: 10.1021/JACS.8B07844.

[4] V. T. Rathod, 'A Review of Acoustic Impedance Matching Techniques for Piezoelectric Sensors and Transducers', *Sensors 2020, Vol. 20, Page 4051*, vol. 20, no. 14, p. 4051, Jul. 2020, doi: 10.3390/S20144051.

[5] M. Tihtih *et al.*, 'Structural, optical, and electronic properties of barium titanate: experiment characterisation and first-principles study', *Materials Technology*, pp. 1–11, Aug. 2022, doi: 10.1080/10667857.2022.2107473.

[6] J. Liu, G. Jin, Y. Chen, and W. Xue, 'Properties of yttrium-doped barium titanate ceramics with positive temperature coefficient of resistivity and a novel method to evaluate the depletion layer width', *Ceram Int*, vol. 45, no. 5, pp. 6119–6124, Apr. 2019, doi: 10.1016/J.CERAMINT.2018.12.086.

[7] M. J. Wang *et al.*, 'Doping behaviors of yttrium, zinc and gallium in BaTiO3 ceramics for AC capacitor application', *Journal of Materials Science: Materials in Electronics*, vol. 25, no. 7, pp. 2905–2912, Apr. 2014, doi: 10.1007/S10854-014-1958-3/FIGURES/5.

[8] D. Makovec, Z. Samardžija, and M. Drofenik, 'Solid Solubility of Holmium, Yttrium, and Dysprosium in BaTiO3', *Journal of the American Ceramic Society*, vol. 87, no. 7, pp. 1324–1329, Jul. 2004, doi: 10.1111/J.1151-2916.2004.TB07729.X.

[9] M. Tihtih, J. E. F. M. Ibrahim, E. Kurovics, and L. A. Gömze, 'Study of the Structure, Microstructure and Temperature Dependent Thermal Conductivity Properties of SrTiO3: Via Y3+ Substitution', *Journal of Nano Research*, vol. 69, pp. 33–42, 2021, doi: 10.4028/WWW.SCIENTIFIC.NET/JNANOR.69.33.

[10] A. Belous, O. V'yunov, L. Kovalenko, and D. Makovec, 'Redox processes in highly yttrium-doped barium titanate', *J Solid State Chem*, vol. 178, no. 5, pp. 1367–1375, May 2005, doi: 10.1016/J.JSSC.2005.01.014.

[11] P. Cavaliere, B. Sadeghi, and A. Shabani, 'Spark Plasma Sintering: Process Fundamentals', *Spark Plasma Sintering of Materials*, pp. 3–20, 2019, doi: 10.1007/978-3-030-05327-7_1.

[12] M. Fattahi, M. Najafi Ershadi, M. Vajdi, F. Sadegh Moghanlou, A. Sabahi Namini, and M. Shahedi Asl, 'On the simulation of spark plasma sintered TiB2 ultra high temperature ceramics: A numerical approach', *Ceram Int*, vol. 46, no. 10, pp. 14787–14795, Jul. 2020, doi: 10.1016/J.CERAMINT.2020.03.003.

[13] R. S. Mahale, V. Shamanth, P. C. Sharath, R. Shashanka, and K. Hemanth, 'A review on spark plasma sintering of duplex stainless steels', *Mater Today Proc*, vol. 45, pp. 138–144, Jan. 2021, doi: 10.1016/J.MATPR.2020.10.357.

[14] E. Ghasali, P. Sangpour, A. Jam, H. Rajaei, K. Shirvanimoghaddam, and T. Ebadzadeh, 'Microwave and spark plasma sintering of carbon nanotube and graphene reinforced aluminum matrix composite', *Archives of Civil and Mechanical Engineering 2018 18:4*, vol. 18, no. 4, pp. 1042–1054, Mar. 2018, doi: 10.1016/J.ACME.2018.02.006.

[15] Z. Cheng and J. Lin, ‘Layered organic-inorganic hybrid perovskites: Structure, optical properties, film preparation, patterning and templating engineering’, *CrystEngComm*, vol. 12, no. 10, pp. 2646–2662, 2010, doi: 10.1039/c001929a.
[16] ‘Synthesis, Properties and Mineralogy of Important Inorganic Materials - Terence E. Warner - Google Books’. Accessed: Jul. 01, 2020. [Online]. Available: https://books.google.hu/books?hl=en&lr=&id=IR_IxoBT_S4C&oi=fnd&pg=PR7&dq=%5B20%5D%09T.E.+Warner,+Synthesis,+properties+and+mineralogy+of+important+inorganic+materials,+John+Wiley+%26+Sons,+2012.&ots=sX5saiM-0W&sig=qnU6Hc6AdLy_ZdJ0FVenAumknko&redir_esc=y#v
[17] O. Bohnke, C. Bohnke, and J. L. Fourquet, ‘Mechanism of ionic conduction and electrochemical intercalation of lithium into the perovskite lanthanum lithium titanate’, *Solid State Ion*, vol. 91, no. 1–2, pp. 21–31, 1996, doi: 10.1016/s0167-2738(96)00434-1.
[18] G. A. Samara, ‘Pressure and temperature dependence of the dielectric properties and phase transitions of the ferroelectric perovskites: Pbtio3 and batio3’, *Ferroelectrics*, vol. 2, no. 1, pp. 277–289, 1971, doi: 10.1080/00150197108234102.
[19] M. R. Ghazanfari, R. Amini, S. F. Shams, M. Alizadeh, and H. A. Ardakani, ‘Effect of mechanical alloying synthesis process on the dielectric properties of (Bi0.5Na0.5)0.94Ba0.06TiO3 piezoceramics’, *Mater Res Bull*, vol. 68, pp. 260–266, 2015, doi: 10.1016/j.materresbull.2015.03.047.
[20] P. Muralt, R. G. Polcawich, and S. Trolier-McKinstry, ‘Piezoelectric thin films for sensors, actuators, and energy harvesting’, *MRS Bull*, vol. 34, no. 9, pp. 658–664, Sep. 2009, doi: 10.1557/mrs2009.177.
[21] Z. Peng and Y. Chen, ‘Preparation of BaTiO3 nanoparticles in aqueous solutions’, in *Microelectronic Engineering*, Apr. 2003, pp. 102–106. doi: 10.1016/S0167-9317(03)00032-7.
[22] A. Habib, R. Haubner, and N. Stelzer, ‘Effect of temperature, time and particle size of Ti precursor on hydrothermal synthesis of barium titanate’, *Mater Sci Eng B Solid State Mater Adv Technol*, vol. 152, no. 1–3, pp. 60–65, Aug. 2008, doi: 10.1016/j.mseb.2008.06.018.
[23] K. M. Hung, W. D. Yang, and C. C. Huang, ‘Preparation of nanometer-sized barium titanate powders by a sol-precipitation process with surfactants’, *J Eur Ceram Soc*, vol. 23, no. 11, pp. 1901–1910, 2003, doi: 10.1016/S0955-2219(02)00431-4.
[24] Y. Hayashi, T. Kimura, and T. Yamaguchi, ‘Preparation of rod-shaped BaTiO3 powder’, *J Mater Sci*, vol. 21, no. 3, pp. 757–762, Mar. 1986, doi: 10.1007/BF01117350.
[25] Y. W. Cho, S. K. Choi, and G. Venkata Rao, ‘The influence of an extrinsic interfacial layer on the polarization of sputtered BaTi O3 film’, *Appl Phys Lett*, vol. 86, no. 20, pp. 1–3, May 2005, doi: 10.1063/1.1921358.
[26] H. Xu, L. Gao, and J. Guo, ‘Hydrothermal Synthesis of Tetragonal Barium Titanate from Barium Chloride and Titanium Tetrachloride under Moderate Conditions’, *Journal of the American Ceramic Society*, vol. 85, no. 3, pp. 727–729, 2004, doi: 10.1111/j.1151-2916.2002.tb00163.x.
[27] C. S. Kim *et al.*, ‘Synthesis and particle size effect on the phase transformation of nanocrystalline TiO2’, *Materials Science and Engineering C*, vol. 27, no. 5-8 SPEC. ISS., pp. 1343–1346, Sep. 2007, doi: 10.1016/j.msec.2006.12.006.
[28] B. J. Chen, E. Y. B. Pun, and H. Lin, ‘Photoluminescence and spectral parameters of Eu3+ in sodium-aluminum-tellurite ceramics’, *J Alloys Compd*, vol. 479, no. 1–2, pp. 352–356, Jun. 2009, doi: 10.1016/j.jallcom.2008.12.072.
[29] S. C. Erwin, L. Zu, M. I. Haftel, A. L. Efros, T. A. Kennedy, and D. J. Norris, ‘Doping semiconductor nanocrystals’, *Nature*, vol. 436, no. 7047, pp. 91–94, Jul. 2005, doi: 10.1038/nature03832.
[30] D. J. Norris, A. L. Efros, and S. C. Erwin, ‘Doped nanocrystals’, *Science (1979)*, vol. 319, no. 5871, pp. 1776–1779, 2008, doi: 10.1126/science.1143802.

[31] K. G. Stamplecoskie, L. Ju, S. S. Farvid, and P. V. Radovanovic, ‘General control of transition-metal-doped GaN nanowire growth: Toward understanding the mechanism of dopant incorporation’, *Nano Lett*, vol. 8, no. 9, pp. 2674–2681, Sep. 2008, doi: 10.1021/nl8009523.

[32] J. Niittynen, R. Abbel, M. Mäntysalo, J. Perelaer, U. S. Schubert, and D. Lupo, ‘Alternative sintering methods compared to conventional thermal sintering for inkjet printed silver nanoparticle ink’, *Thin Solid Films*, vol. 556, pp. 452–459, Apr. 2014, doi: 10.1016/J.TSF.2014.02.001.

[33] H. Pastor, ‘Metallic Borides: Preparation of Solid Bodies — Sintering Methods and Properties of Solid Bodies’, *Boron and Refractory Borides*, pp. 457–493, 1977, doi: 10.1007/978-3-642-66620-9_25.

[34] M. A. Awotunde, A. O. Adegbenjo, B. A. Obadele, M. Okoro, B. M. Shongwe, and P. A. Olubambi, ‘Influence of sintering methods on the mechanical properties of aluminium nanocomposites reinforced with carbonaceous compounds: A review’, *Journal of Materials Research and Technology*, vol. 8, no. 2, pp. 2432–2449, Apr. 2019, doi: 10.1016/J.JMRT.2019.01.026.

[35] Z. H. Zhang, Z. F. Liu, J. F. Lu, X. B. Shen, F. C. Wang, and Y. D. Wang, ‘The sintering mechanism in spark plasma sintering – Proof of the occurrence of spark discharge’, *Scr Mater*, vol. 81, pp. 56–59, Jun. 2014, doi: 10.1016/J.SCRIPTAMAT.2014.03.011.

[36] Y. Slimani, A. Selmi, E. Hannachi, M. A. Almessiere, A. Baykal, and I. Ercan, ‘Impact of ZnO addition on structural, morphological, optical, dielectric and electrical performances of BaTiO3 ceramics’, *Journal of Materials Science: Materials in Electronics*, vol. 30, no. 10, pp. 9520–9530, May 2019, doi: 10.1007/S10854-019-01284-2/FIGURES/10.

[37] M. Tihtih, J. E. F. M. Ibrahim, E. Kurovics, and L. A. Gömze, ‘Synthesis of Ba1−xSrxTiO3 (x = 0–0.3) Ceramic Powders via Sol-Gel Method: Structural, Microstructure, Thermal Conductivity, and Compressive Strength Properties’, *Crystal Research and Technology*, p. 2100106, Oct. 2021, doi: 10.1002/CRAT.202100106.

[38] J. Liu, G. Jin, Y. Chen, and W. Xue, ‘Properties of yttrium-doped barium titanate ceramics with positive temperature coefficient of resistivity and a novel method to evaluate the depletion layer width’, *Ceram Int*, vol. 45, no. 5, pp. 6119–6124, Apr. 2019, doi: 10.1016/J.CERAMINT.2018.12.086.

[39] C. H. Kim, K. J. Park, Y. J. Yoon, M. H. Hong, J. O. Hong, and K. H. Hur, ‘Role of yttrium and magnesium in the formation of core-shell structure of BaTiO3 grains in MLCC’, *J Eur Ceram Soc*, vol. 28, no. 6, pp. 1213–1219, Jan. 2008, doi: 10.1016/J.JEURCERAMSOC.2007.09.042.

[40] M. Tihtih, J. F. M. Ibrahim, E. Kurovics, and M. Abdelfattah, ‘Study on the effect of Bi dopant on the structural and optical properties of BaTiO3 nanoceramics synthesized via sol-gel method’, *J Phys Conf Ser*, vol. 1527, no. 1, 2020, doi: 10.1088/1742-6596/1527/1/012043.

[41] M. Tihtih *et al.*, ‘Role of A-site (Sr), B-site (Y), and A, B sites (Sr, Y) substitution in lead-free BaTiO3 ceramic compounds: Structural, optical, microstructure, mechanical, and thermal conductivity properties’, *Ceram Int*, vol. 49, no. 2, pp. 1947–1959, Jan. 2023, doi: 10.1016/J.CERAMINT.2022.09.160.

[42] M. Tihtih *et al.*, ‘Enhanced optical and thermal conductivity properties of barium titanate ceramic via strontium doping for thermo-optical applications’, *Opt Quantum Electron*, vol. 55, no. 3, pp. 1–20, Mar. 2023, doi: 10.1007/S11082-022-04516-8/TABLES/3.

[43] K. S. Park, ‘Structural and electrical properties of FeMg0.7Cr0.6Co0.7−xAlxO4 ($0 \leq x \leq 0.3$) thick film NTC thermistors’, *J Eur Ceram Soc*, vol. 26, no. 6, pp. 909–914, Jan. 2006, doi: 10.1016/J.JEURCERAMSOC.2004.12.021.

[44] C. Pascual-Gonzalez *et al.*, ‘Continuously controllable optical band gap in orthorhombic ferroelectric KNbO3-BiFeO3 ceramics’, *Appl Phys Lett*, vol. 110, no. 17, p. 172902, Apr. 2017, doi: 10.1063/1.4982600.

[45] C. Pascual-Gonzalez *et al.*, ‘Band gap evolution and a piezoelectric-to-electrostrictive crossover in (1 − x)KNbO 3 – x (Ba 0.5 Bi 0.5)(Nb 0.5 Zn 0.5)O 3 ceramics’, *J Mater Chem C Mater*, vol. 5, no. 8, pp. 1990–1996, Feb. 2017, doi: 10.1039/C6TC05515J.

[46] W. Zhou, H. Deng, L. Yu, P. Yang, and J. Chu, ‘Magnetism switching and band-gap narrowing in Ni-doped PbTiO3 thin films’, *J Appl Phys*, vol. 117, no. 19, p. 194102, May 2015, doi: 10.1063/1.4921459.

[47] R. Yin, Y. Zhang, W. Zhao, X. Huang, X. Li, and L. Qian, ‘Graphene platelets/aluminium nitride metacomposites with double percolation property of thermal and electrical conductivity’, *J Eur Ceram Soc*, vol. 38, no. 14, pp. 4701–4706, Nov. 2018, doi: 10.1016/J.JEURCERAMSOC.2018.06.036.

[48] J. Suchanicz, P. Czaja, K. Kluczewska, H. Czternastek, M. Sokolowski, and A. Węgrzyn, ‘The Influence of Pb(Mg1/3Nb2/3)O3-doping on the thermoelectric properties of BaTiO3 ceramics’, *https://doi.org/10.1080/01411594.2018.1506880*, vol. 91, no. 9–10, pp. 1036–1043, Oct. 2018, doi: 10.1080/01411594.2018.1506880.

[49] X. Xiao *et al.*, ‘Tailoring the structure and thermoelectric properties of BaTiO3via Eu2+ substitution’, *Physical Chemistry Chemical Physics*, vol. 19, no. 21, pp. 13469–13480, May 2017, doi: 10.1039/C7CP00020K.

[50] C. J. Xiao, ‘A study on the damping capacity of BaTiO3-reinforced Al-matrix composites’, *Bulletin of Materials Science*, vol. 39, no. 2, pp. 463–467, Apr. 2016, doi: 10.1007/S12034-016-1171-5/FIGURES/7.

[51] T. Badapanda *et al.*, ‘Optical and dielectric study of strontium modified barium zirconium titanate ceramic prepared by high energy ball milling’, *J Alloys Compd*, vol. 645, pp. 586–596, Oct. 2015, doi: 10.1016/J.JALLCOM.2015.05.005.

[52] Z. Yang *et al.*, ‘Grain size engineered lead-free ceramics with both large energy storage density and ultrahigh mechanical properties’, *Nano Energy*, vol. 58, pp. 768–777, Apr. 2019, doi: 10.1016/J.NANOEN.2019.02.003.

[53] C. N. Berglund and H. J. Braun, ‘Optical Absorption in Single-Domain Ferroelectric Barium Titanate’, *Physical Review*, vol. 164, no. 2, p. 790, Dec. 1967, doi: 10.1103/PhysRev.164.790.

[54] Z. Yu and C. Ang, ‘Maxwell–Wagner polarization in ceramic composites BaTiO3–(Ni0.3Zn0.7)Fe2.1O4’, *J Appl Phys*, vol. 91, no. 2, pp. 794–797, Jan. 2002, doi: 10.1063/1.1421033.

[55] A. Rached, M. A. Wederni, K. Khirouni, S. Alaya, R. J. Martín-Palma, and J. Dhahri, ‘Structural, optical and electrical properties of barium titanate’, *Mater Chem Phys*, vol. 267, p. 124600, Jul. 2021, doi: 10.1016/J.MATCHEMPHYS.2021.124600.

[56] M. Tyunina, ‘Conductivity in Ferroelectric Barium Titanate: Electrons Versus Oxygen Vacancies’, *IEEE Trans Ultrason Ferroelectr Freq Control*, vol. 68, no. 2, pp. 296–302, Feb. 2021, doi: 10.1109/TUFFC.2020.2978901.

[57] C. Deng *et al.*, ‘Spark plasma sintered graphene/copper calcium titanate ceramic composites with negative permittivity and enhanced thermal conductivity’, *Ceram Int*, vol. 49, no. 10, pp. 16149–16155, May 2023, doi: 10.1016/J.CERAMINT.2023.01.212.